Technical and Economic Feasibility of Crushed Rock with Synthetic Oil Heat Storage Coupled to Light Water Reactors in the United Arab Emirates

By

Ali Saleh Aljefri

B.S., Nuclear Engineering (2014) The Pennsylvania State University

SUBMITTED TO THE
DEPARTMENT OF NUCLEAR SCIENCE AND ENGINEERING

IN PARTIAL FULFILLMENT OF THE REQUIREMENTS FOR THE DEGREE OF
MASTER OF SCIENCE IN NUCLEAR SCIENCE AND ENGINEERING

AT THE
MASSACHUSETTS INSTITUTE OF TECHNOLOGY
SEPTEMBER 2021

© 2021 Massachusetts Institute of Technology
All rights reserved.

Signature of Author: _____
Ali Saleh Aljefri
Department of Nuclear Science and Engineering
August 9, 2021

Certified by: _____
Charles W. Forsberg
Principal Research Scientist of Nuclear Science and Engineering
Thesis Supervisor

Certified by: _____
Jacopo Buongiorno
TEPCO Professor of Nuclear Science and Engineering
Thesis Reader

Accepted by: _____
Ju Li
Battelle Energy Alliance Professor of Nuclear Science and Engineering
and Professor of Materials Science and Engineering
Chair, Department Committee on Graduate Students

Technical and Economic Feasibility of Crushed Rock with Synthetic Oil Heat Storage Coupled to Light Water Reactors in the United Arab Emirates

by

Ali Saleh Aljefri

Submitted to the department of Nuclear Science and Engineering on
August 9, 2021, in partial fulfillment of the requirements for the degree of
Master of Science in Nuclear Science and Engineering

Abstract

The United Arab Emirates (UAE) has the goal to reduce greenhouse gas emissions from the electricity sector. The UAE is building four pressurized-water reactors and expanding solar generation. Large-scale addition of solar without storage results in excess capacity and inefficient dispatch during some periods of the year. Adding heat storage to the nuclear power plants was investigated to reduce electricity generation at times of excess solar generation and provide added electricity at times of no solar output while the reactors are operated at baseload. This results in full utilization of nuclear and higher utilization of solar while reducing carbon dioxide emission from fossil plants. A new low-cost heat storage is proposed to address the storage needs—the Crushed Rock Ultra-large Stored Heat (CRUSH) system. CRUSH enables low-cost 100-GWh of heat storage to address daily to weekday/weekend heat storage needs. The performance of the grid and the performance of CRUSH were analyzed to understand total system performance and explore the option space for the design.

Thesis Supervisor: Charles W. Forsberg
Title: Principal Research Scientist of Nuclear Science and Engineering

Thesis Reader: Jacopo Buongiorno
Title: TEPCO Professor of Nuclear Science and Engineering

Acknowledgments

I would like to express my heartfelt gratitude to my thesis supervisor, Dr. Charles Forsberg, for giving me the opportunity to work with him. Without his continuous support this work would not have been possible. I would like to extend my deepest appreciation to my thesis reader, Professor Jacopo Buongiorno, for his guidance through this thesis and for his valuable input and feedback.

This thesis would not have been possible without the collaboration and help from my dear friends Dr. Abdulla Alhajri and Abdulla Alkatheri. I would like to thank EWEC and TRANSCO for their support and showing no hesitation in providing crucial data for this work to be complete.

To my parents, there will never be enough words to express my love and gratitude to you. You have always been a source of inspiration and support through my career. I would like to thank my brothers and sisters who have always been by my side. I would like to thank my friends in the UAE and Boston for being there when I need them.

I would like to thank the NSE department for an experience of a lifetime. Special thanks to Brandy Baker, Heather Barry, Peter Brenton, and Teva Ragule. You really made my life easier in this difficult year of COVID-19.

I am exceptionally grateful to my country the UAE and to the Emirates Nuclear Energy Corporation (ENEC) for giving me this opportunity. Namely Dr. Ausaf Hussein who believed in me and supported me through my early career. I would like to thank Mr. Mohamed Alhammadi and Dr. Mohamed Chookah for supporting me and giving me this opportunity.

Table of Contents

List of Figures

List of Tables

1. Introduction

1.1 Motivation

Historically most nuclear plants produced base-load electricity while fossil-fuel plants produced variable electricity. This has been the most economic system because nuclear power plants have high capital costs and low operating costs while fossil fuel plants have lower-capital costs and higher operating costs. The goal of a low-carbon energy system requires a replacement of fossil fuel plants in the role of providing variable dispatchable electricity. Base-load nuclear plants with heat storage have the potential to economically replace fossil fuels in their role of providing dispatchable electricity.

Wind and solar in good locations provide low-cost electricity at times of high wind and solar output but cannot provide assured generating capacity. The large-scale addition of solar results in collapse of wholesale electricity prices in the middle of the day with higher prices before sunrise and as the sun goes down as shown in Figure 1. In these markets, there are large incentives to couple heat storage to nuclear power plants to enable base-load nuclear plants to produce variable electricity and increase revenue by selling more electricity when prices are high and avoid selling electricity when prices are near zero. While storage adds energy inefficiencies to the power cycle, storage can improve the economics.

Figure 1. California Wholesale Electricity Prices, March 31, 2019, with Midday Price Collapse

1.2 Thesis Organization

This thesis consists of four major parts. The first part (Chapter 2) identifies the incentives of utilizing heat storage with nuclear energy in the UAE and assesses the potential markets that can benefit economically from the heat stored by nuclear energy in the UAE. The second part (Chapters 3&5) explores the current technology options for nuclear heat storage and proposes a novel low-cost crushed rock heat storage system, CRUSH. The third part (Chapter 4) utilizes capacity expansion modeling tools, GenX, to assess the economic benefits from coupling heat storage to nuclear reactors in the UAE. The last part (Chapter 6) is an engineering analysis using a numerical model developed to explore the behavior and option space of CRUSH system.

2. Energy Markets and the UAE

The United Arab Emirates have excellent solar resources, have an electricity grid built on fossil fuels and is constructing four large nuclear power plants. This section describes the UAE electricity sector and the goal to reduce carbon emissions that creates the incentives to consider adding heat storage to the four nuclear plants to provide variable electricity to the grid. While the analysis is specific to the UAE, other parts of the middle east and parts of the American southwest have similar situations.

2.1 The Energy Sector in the UAE

Energy resources are not well diversified in the UAE with oil and natural gas accounting for around 99% of the primary energy resources (IRENA, 2019). Nonetheless, the government of the UAE is in the process of diversifying energy resources mainly through the deployment of nuclear and solar energy. Electricity generation accounts for 19% of the energy consumption in the UAE. Transportation accounts for 22%. Industrial heat is the largest sector of energy consumption in the UAE accounting for 59% (IRENA, 2015). Due to the rapid growth in population, energy demand grows rapidly in the UAE (Orhan et al., 2016). For the years 2006-2016, the annualized growth in electricity consumption in the UAE was about 7% compared to 4% worldwide. Furthermore, energy use per capita in the UAE is higher than industrialized countries such as the US, Japan, and Germany (IRENA, 2019). The growing energy demand in the UAE comes with two challenges that need to be tackled to sustain the economic development cycle that are addressed herein: meeting climate change goals and insuring energy security of supply.

2.2 Climate Change Goals and Reducing Carbon Emissions

The UAE has one of the highest CO_2 emissions per capita in the world. According to the world bank data in 2014, the UAE ranked 6th worldwide with 22.9 metric tons of CO_2 per capita

(World Bank, 2014). Figure 2 shows the growing total carbon emissions in the UAE throughout the years. The increase in carbon emissions is due to the rapid growth in population and energy consumption coupled with continuous addition of fossil fuel installed capacity.

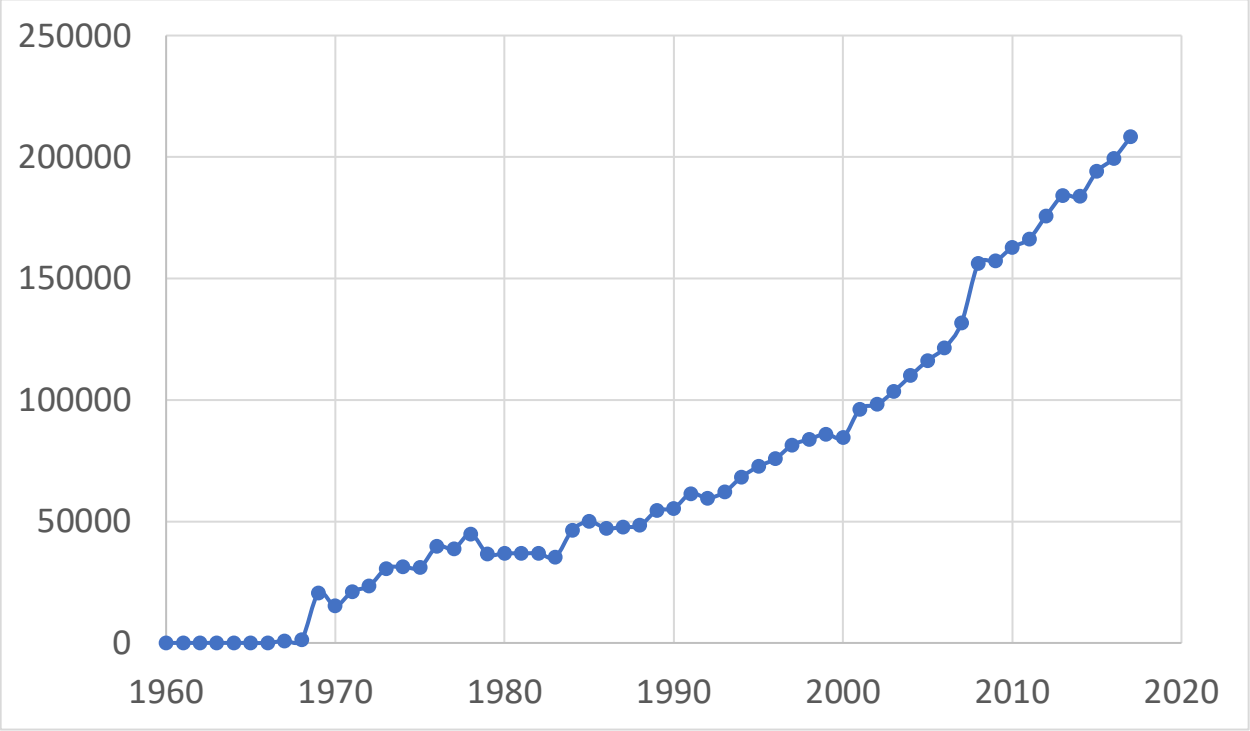

Figure 2. Yearly CO2 emissions in kilotons in the UAE (Source: World Bank)

In 2015, the UAE has joined 195 countries in the Paris Agreement that limits temperature increase below 2°C (Awad, 2018). The UAE has committed to lower carbon emissions through several initiatives. The most important being the UAE Energy Strategy 2050 launched in 2015. This strategy targets 50% clean energy consisting of 44% renewables and 6% nuclear, that is the total energy not just the electricity sector. It is clear that the main driver in lowering carbon emissions through this strategy is the deployment of renewable energy sources, primarily solar energy. The successful implementation of this strategy could reduce carbon emissions by 70% (Awad, 2018) from the electricity sector. Figure 3 shows the potential reductions on carbon emissions in the UAE in a scenario of 25% renewable energy capacity in 2030. Nevertheless,

previous experience in the UAE has shown difficulty in meeting solar energy deployment targets. For example, the emirate of Abu Dhabi has committed to installing 7% of total installed capacity from renewable sources by 2020 (IRENA, 2019). However, in a recent report launched by Abu Dhabi Transmission and Dispatch Company, the forecasted energy portfolio of the emirate in 2025 is expected to have 4.4% installed capacity from renewables (Transco, 2018). The discrepancy between the target and actual solar energy installed is due to the intermittency of solar energy penetration and the lack of electricity storage capabilities.

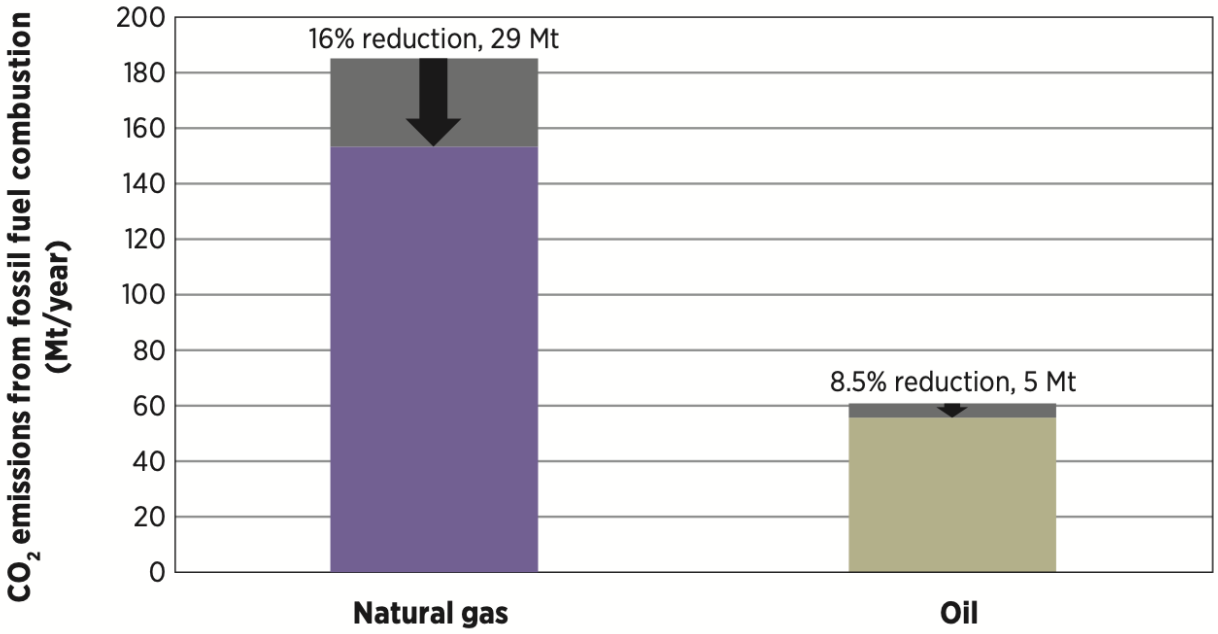

Figure 3. Potential reduction in CO_2 emissions with renewable energy implementation (Source: IRENA 2015)

2.3 Energy Security of Supply and Independence

Another challenge that faces the energy sector in the UAE is achieving energy independence. The UAE depends heavily in natural gas to produce electricity and to power heavy industries including petrochemicals, aluminum, and steel (IRENA, 2019). Figure 4 shows the breakdown of natural gas consumption in the UAE. The natural gas produced locally comes from

the gas associated with oil wells (Sgouridis, 2013). Even though the UAE has large reserves of natural gas, in 2008 the UAE became a net natural gas importer to satisfy the shortage in natural gas production (IRENA, 2019). The reason to import natural gas is that the local natural gas in the UAE has high content of Sulphur that requires expensive processing to remove before use. If the UAE decided to produce gas from high Sulphur wells regardless of the cost, the cost of natural gas will increase more than 400% compared to the cost of producing gas in 2009 (IRENA, 2015).

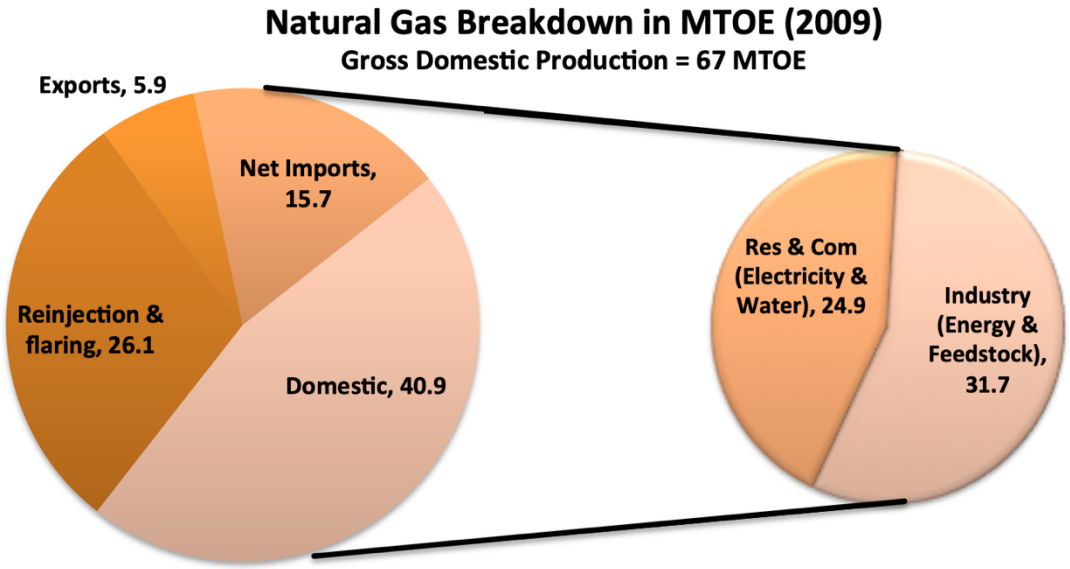

Figure 4. Natural Gas production and consumption in the UAE (Source: Sgouridis, 2013)

The UAE imports natural gas from the neighboring country Qatar through the Dolphin pipeline. The UAE signed an agreement with Qatar in 2010 to supply gas through 2032 with a fixed price of USD 2/MBtu (IRENA, 2015). Depending on imported natural gas to meet energy demands puts the country in a jeopardized situation. Energy is a matter of national security and having the main source of energy practically controlled by neighboring country is not on the best interest of the national security of the UAE. Furthermore, the favorable terms in the agreement end

in 2032 and it is very unlikely to renew the contract with the same favorable terms specially if the UAE is in a situation where this pipeline is still one of the main sources of energy in the country.

Reducing carbon emissions and insuring energy security of supply and independence are major challenges that faces the energy sector in the UAE. The government is actively looking for solutions to mitigate and solve these challenges. However, the option of utilizing nuclear power in a way other than a source of baseload power has not been investigated in any detail.

2.4 Peak Demand Electricity Market

To understand the case for using heat storage with nuclear energy in the UAE for peak power production, it is important to understand the electricity market in the UAE. The UAE consists of seven emirates each with its own electricity dispatching strategies. Nonetheless, the electric grid connects the seven emirates to allow power transfers between emirates in times of peak demand or shortage of supply. Because of the separate dispatch entities, the data to be analyzed can be extracted for each emirate separately. For the purpose of this paper, the electric grid of the emirate of Abu Dhabi is chosen to be examined for two reasons. First, Abu Dhabi is the largest emirate with the largest electricity demand. The installed capacity in Abu Dhabi constitutes more than 50% of the installed capacity in the UAE (IRENA, 2019 & Transco, 2018). Second, Abu Dhabi has the most diversified sources of electricity with several solar projects online and under construction and nuclear power coming online in the early 2020s. Furthermore, due to the small size of the country, the demand trends that are affected by the weather daily and seasonally are very similar for all emirates.

The demand for electricity in the UAE is growing rapidly reflecting the high growth in GDP. Figure 5 shows the historic and forecasted peak demand in Abu Dhabi for a range of

scenarios. The committed generation capacity consists mainly of a 1 GW solar PV plant and the 5.6 GW from four nuclear reactors (Transco, 2018).

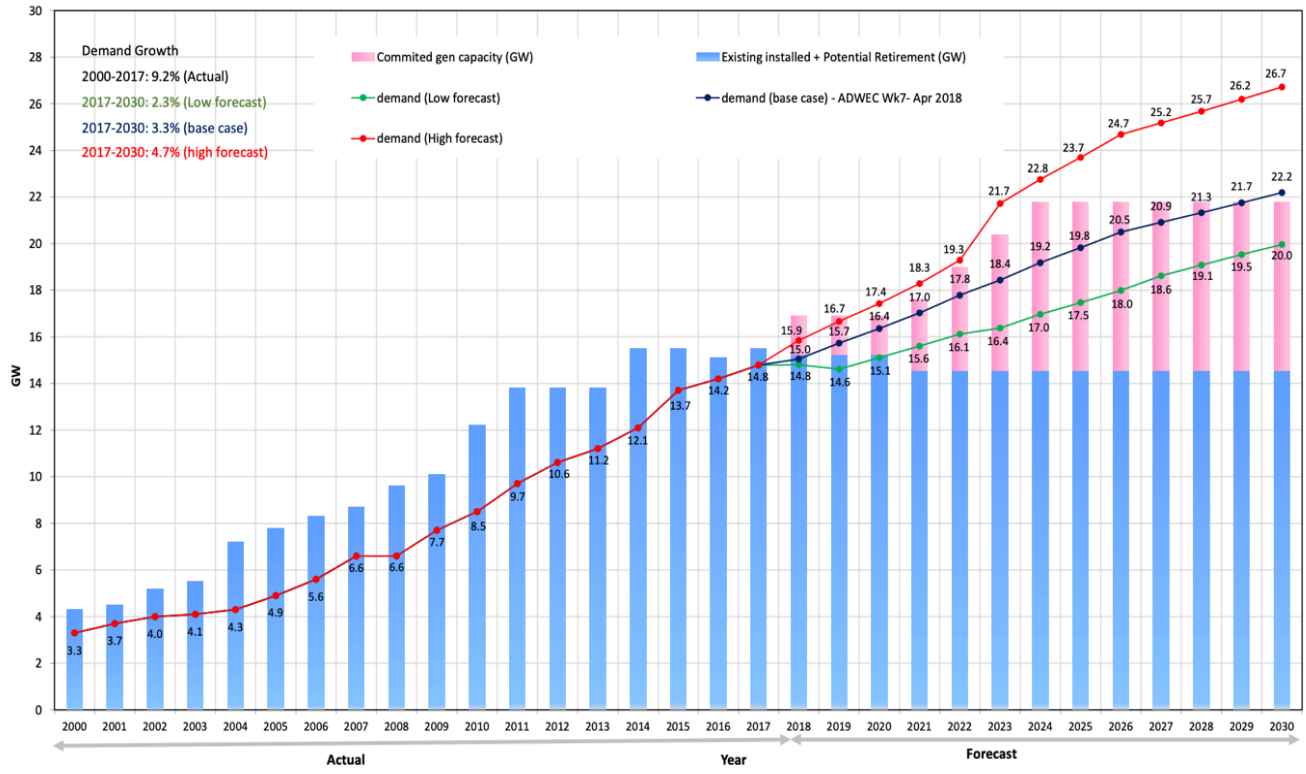

Figure 5. Actual and predicted peak demand in Abu Dhabi (Source: Transco 2018)

There is difficulty in meeting renewable energy deployment targets due to the intermittency of solar power. However, solar power is considered the most promising energy resource in the UAE due to the availability and declining cost (IRENA, 2015). In the yearly planning report published by the Abu Dhabi Transmission and Dispatch Company, solar PV is assumed to have the potential of producing 5.7 GW of average capacity by the year 2030. This scenario is examined throughout the report (Transco, 2018). The difficulty of penetrating vast amounts of solar energy on the system can be understood by examining the daily demand curve and comparing that with the available hours of solar energy as seen in Figure 6. Figure 6 shows the hourly energy demand

and the net generation by technology for the highest demand peak day in the year for the 2030 forecast scenario. It can be seen that solar production aligns with the peak demand in the middle of day and late afternoon. However, the demand stays relatively at the same level throughout the day even during night hours where solar PV does not produce electricity—partly because of the very large air-conditioning loads. This leads to the necessity of having fossil fuel installed capacity to compensate for the hours of solar intermittency regardless of the installed capacity of Solar PV. Figure 7 shows the electricity demand in Abu Dhabi throughout the year for the scenario of 2030 forecast. There is a period of over-generation and inefficient dispatch of solar PV for around 40% of the time of the year. This is mainly due to the days that solar output exceeds the demand during daylight hours.

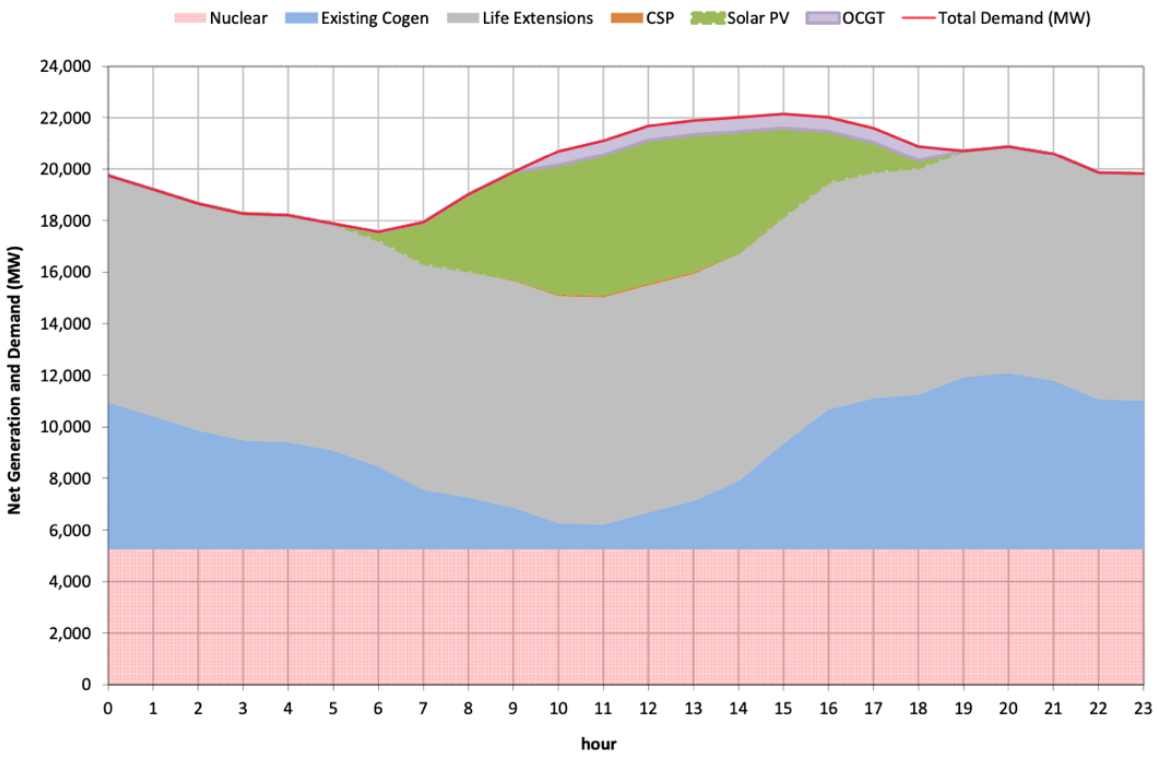

Figure 6. Daily electricity demand in Abu Dhabi 2030 expectation (Source: Transco 2018)

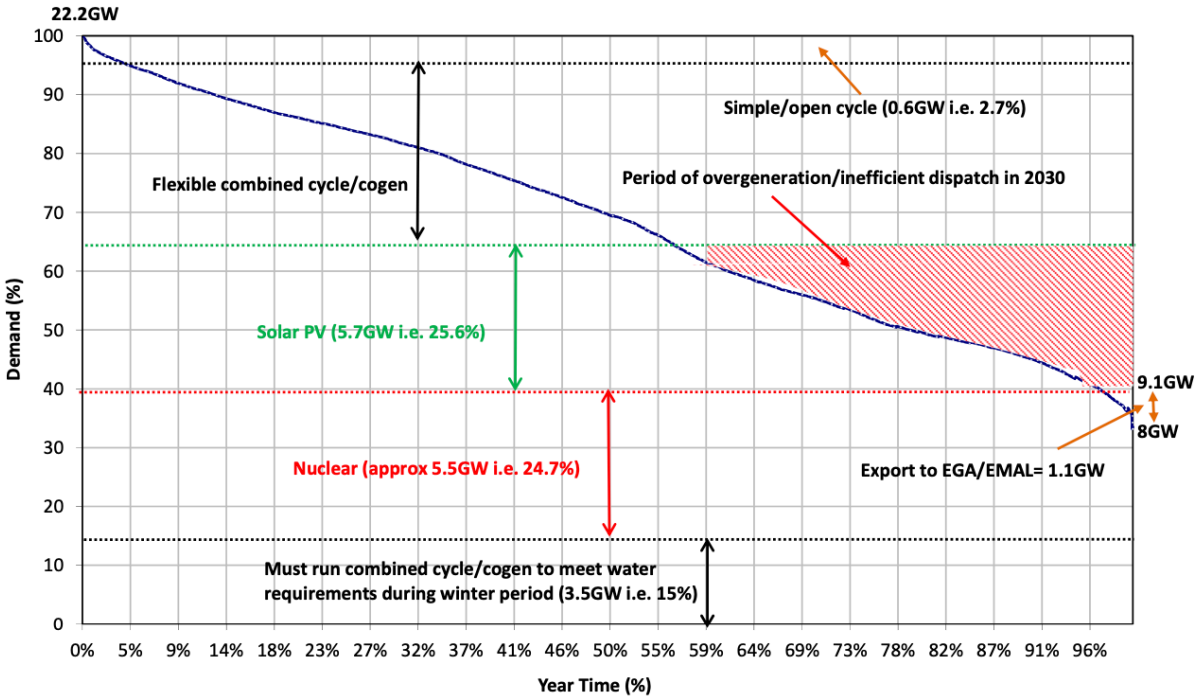

Figure 7. Electricity demand in Abu Dhabi (Source: Transco 2018)

There are two main takeaway messages from analyzing figures 6 and 7. First of all, even though solar energy is a promising future cheap source of electricity in the UAE, its penetration in the UAE grid is hindered by two main factors: (1) the inability of producing energy during nighttime and (2) the inefficient over generation when demand is low. The inefficient utilization of solar power keeps the demand for fossil fuel fuels high which contradicts the goals of reducing carbon emissions and reducing dependency on imported natural gas. Furthermore, gas turbines efficiencies drop when operating at part load. Therefore, producing electricity through gas turbines at times of low solar energy is wasteful and not economically attractive. The second main message from figures 6 and 7 is that nuclear energy coupled with dispatchability capabilities can be used to increase the effectiveness of solar energy and therefore allows for more solar penetration. This will allow for the generation of electricity form Solar PV and Nuclear at their full capacities and reduce fossil fuel consumption.

3. Technology Options for LWR Heat Storage

Nuclear reactors in the UAE are Light Water Reactors (LWRs). Light Water Reactors generate power using a Rankine cycle that utilizes the heat produced in the Reactor Core. To minimize the cost of electricity, the reactor power should be 100% of the time. LWRs can operate at part load. Figure 8 shows the effect of change in reactor power to the efficiency of a nuclear power plant. This is due to the thermodynamics of the Rankine cycle and operating the turbine off its normal optimum operating point. The turbine plant is designed for a specific set of steam conditions. As the power level decreases, efficiency decreases. However, the loss of efficiency is less than 10% from 40% of power to 100% of power. If the steam supply to the turbine is too low, the turbine will trip offline. There is the option to operate the reactor at full power with some steam going to the turbine and the remainder of the steam going to heat storage to be used to generate peak electricity at a different time. Coupling heat storage to nuclear reactors does not affect the steam supply; ensuring that the reactor is running at full power all the time.

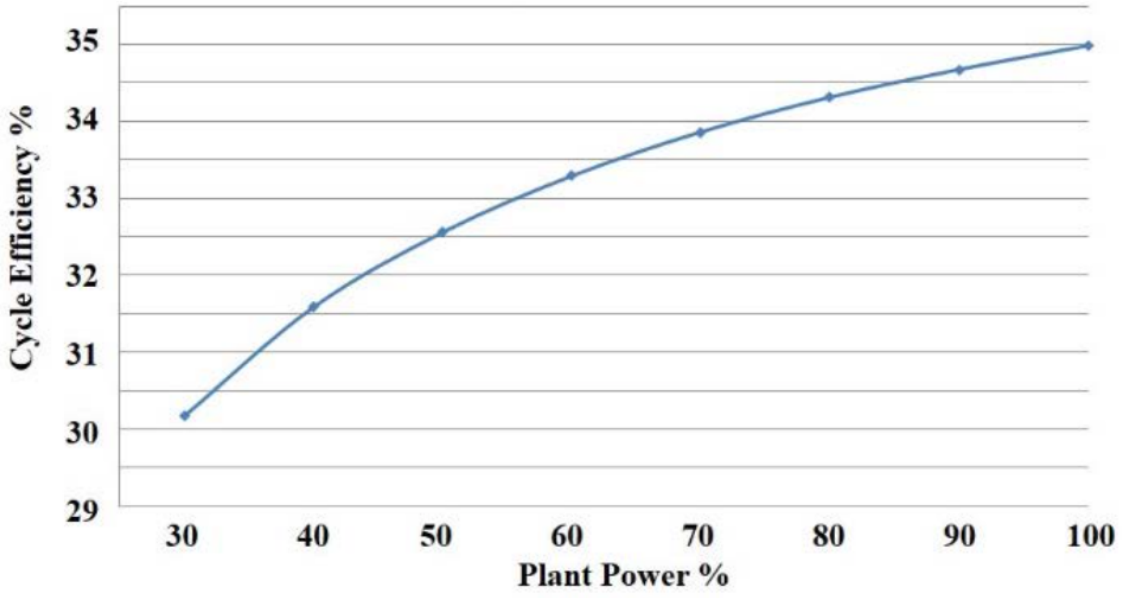

Figure 8. Nuclear Reactor efficiency with power variation (Source: Westinghouse Corporation)

Heat storage can be coupled to nuclear reactors by either a stand-alone storage system or an integrated storage system (Forsberg, 2017). In a stand-alone storage system, the steam removed from the reactor is stored as heat and later used in a separate turbine. In an integrated storage system, the steam diverted from the reactor is stored and then recovered to the reactor turbine (Forsberg, 2017).

There are several technology options to couple nuclear reactors to heat storage. A focused study conducted at MIT in collaboration with Idaho National Lab and Exelon has identified six classes of storage options for LWRs. Three technology options are discussed in this thesis due to their applicability, compatibility, and previous experience with other types of energy production.

3.1 Sensible Heat Storage

Sensible heat storage is very attractive to apply to nuclear power plants because it is already used commercially with concentrated solar power plants (Boardman, 2019). Sensible heat storage utilizes a fluid, typically oils or molten salts, to store heat. The heat stored is then retracted through a heat exchanger and the steam produced is sent to the turbine (Forsberg, 2017). Figure 9 shows the configuration of a sensible heat storage system. Previous studies have indicated that the recovered heat from sensible heat storage is able to produce 20 to 25% more power above the baseload during peak power demand (Forsberg, 2017). Furthermore, coupling nuclear reactors to sensible heat storage results in a 2.5% increase in the capacity factor compared to load following as the reactor thermal output remains nearly constant when heat storage is used for varying the power output (Amuda & Field, 2020).

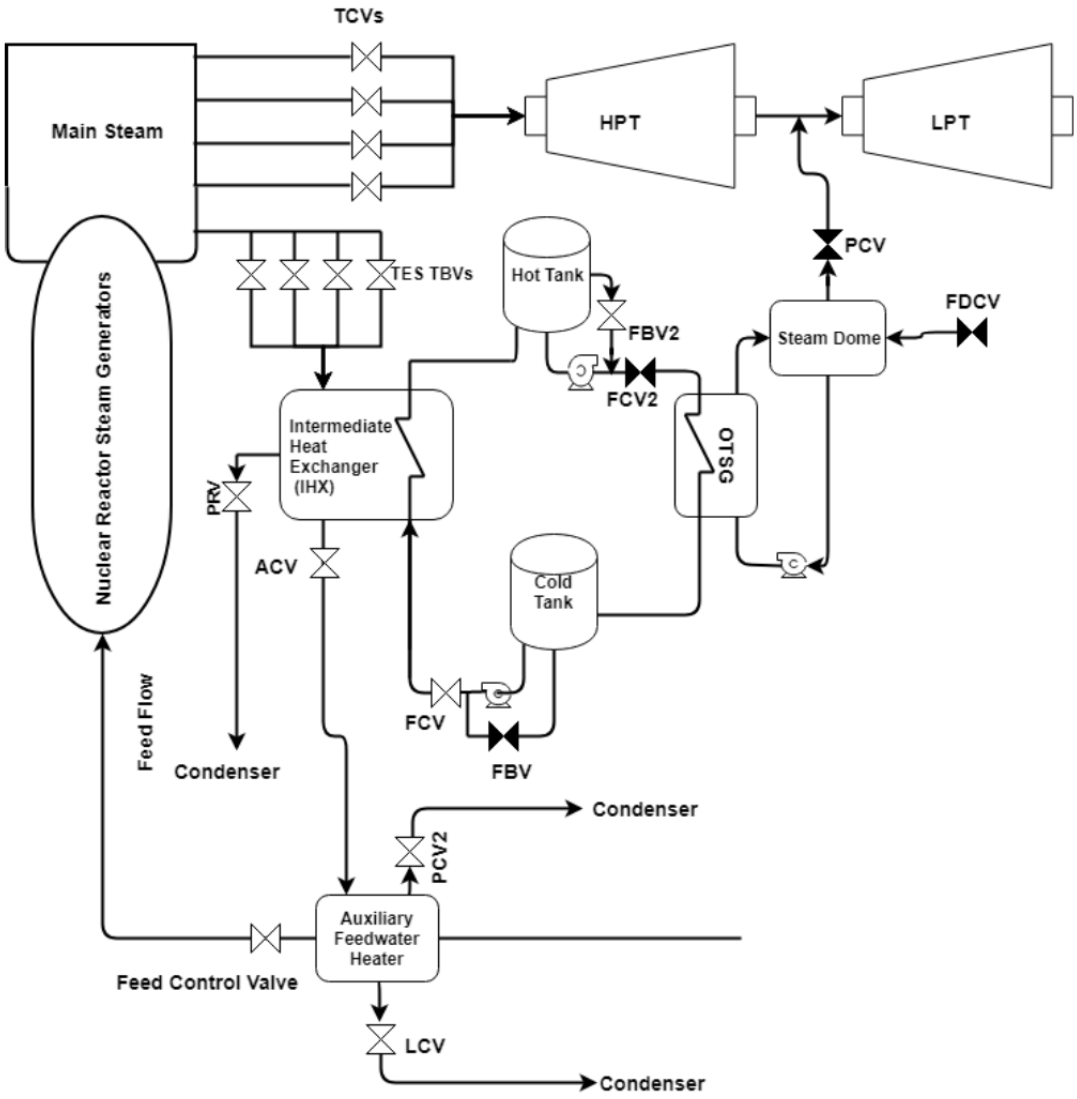

Figure 9. Sensible Heat Storage System (Source: Boardman, 2019)

A special type of sensible heat storage utilizes a packed bed of crushed rock for heat storage. This system is being developed and analyzed by Kepco Internationa Nuclear Gradurate School (KINGS) in South Korea for the APR 1400 reactor. In this system, oil is used as a heat transfer medium that carries the heat from the main steam coming from the reactor. The heat transfer from the main steam to the oil occurs through heat exchangers in the proposed Heat Storage Building (HSB) adjacent to the reactor. The HSB hosts the heat exchangers between steam

and oil to heat up the oil. The hot oil is then transferred to an oil storage tank (OST) that is filled with a packed bed of Hornfel gravels (crushed rock). Crushed rock is chosen for its low cost and high heat capacity. High heat capacity is desirable to minimize volume and thus container costs per unit of heat stored. In the recovery mode, the heat stored in the storage tanks is transferred through the oil to the secondary side feedwater in the Heat Recovery Building (HRB). The HRB hosts the heat exchangers between oil and water to extract heat from the hot oil. Then, steam generated is sent to the turbine building to produce power. Figure 10 demonstrates the proposed design of the storage system (Field et al., 2019). The round-trip efficiency of the proposed sensible heat storage system coupled to APR 1400 ranges from 55 to 75%. A suggested daily cycle comprises of three phases. 8 hours charging at 800 MWth, 14 hours of recovering at 420-450 MWth, and the balance of the day allocated for 2 hours for shifting between charging and recovery modes in both directions (Kluba & Field, 2019). Figure 11 shows a proposed steam cycle paths for the APR 1400 integrated storage system with three options where the steam is recovered to the main turbine hall (Amuda & Fields, 2020). In all three paths heat is stored from high pressure steam exiting the steam generator. The three options differ in the heat recovery path.

- The first option is the recovery of heat through superheated steam supply to the low-pressure turbines.
- The second option is using the recovered heat to supply the shell side of the high-pressure feedwater heaters replacing the extracted steam from the high-pressure turbine that were used for the feedwater heaters.
- The third option is to recover heat as a direct supply of feedwater which in turn reduces the required extracted steam from the high-pressure turbine to supply the feedwater heaters.

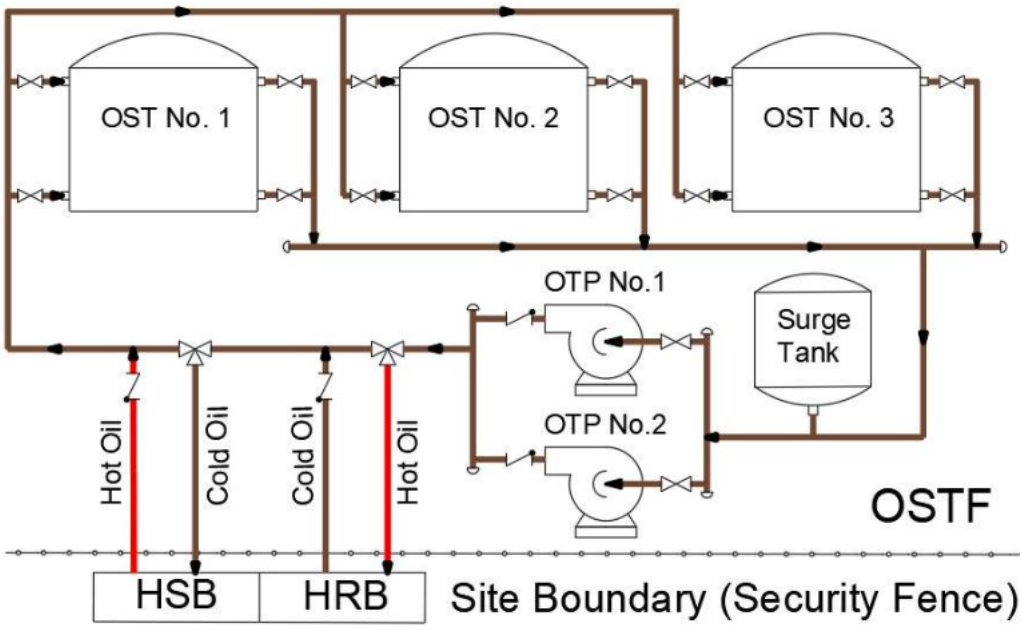

Figure 10. Sensible Heat Storage with Crushed Rock for APR 1400 (Field et al., 2019)

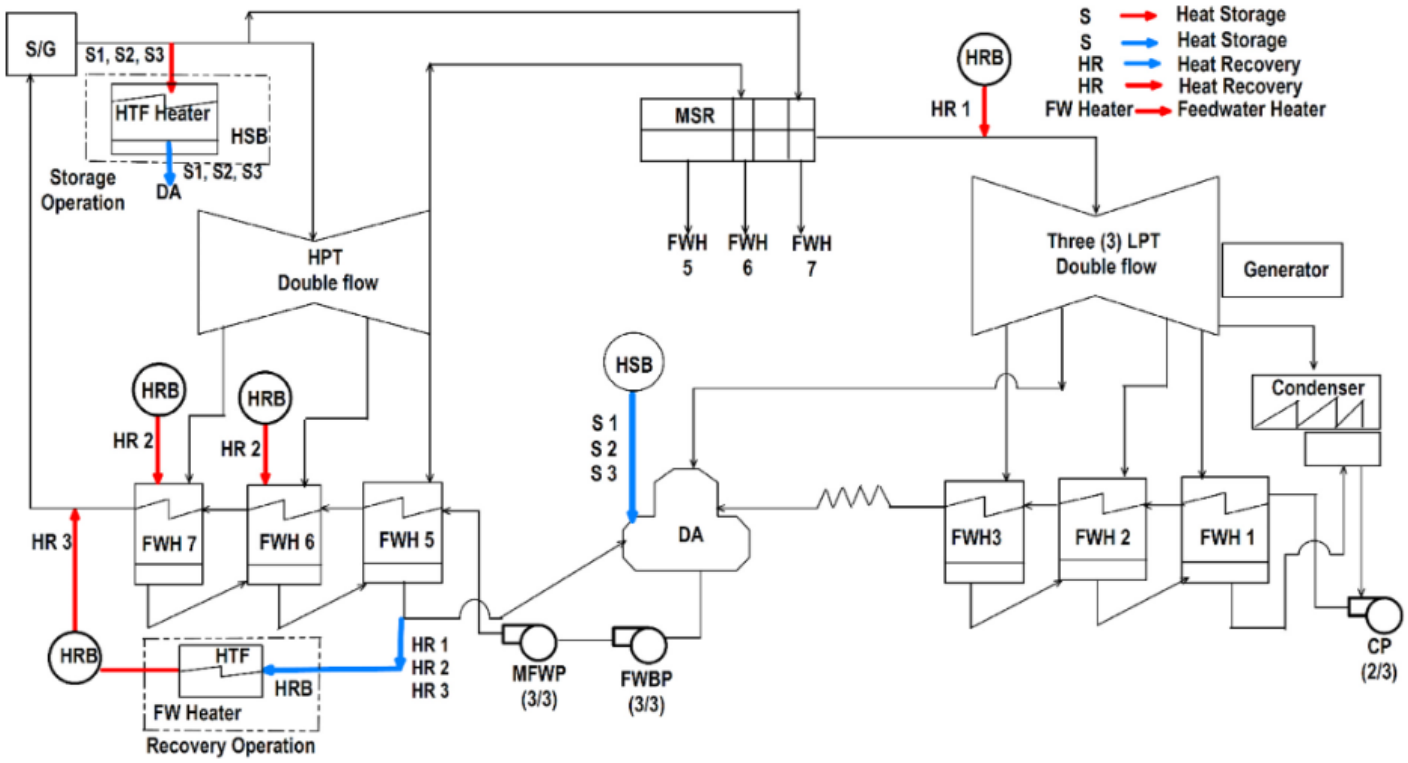

Figure 11. APR1400 integrated storage system (Source: Amuda & Field, 2020)

A major consideration in the KINGS design of the APR 1400 heat storage system is reducing the required modifications to the plant design. Removing steam before it goes to the turbine building and then returning it to the turbine building introduces operational challenges in terms of reactor power control during transition periods from charging and recovery modes. To reduce the required design modifications, the proposed design by KINGS university limits the steam extracted from the reactor to 20% of the total produced steam (Field, 2019). The heat coming back from heat storage is used to provide feed-water heating—not back to the turbines that would require greater modifications of the steam plant.

3.2 Steam Accumulators

Steam accumulators is another storage technology that is commercially used. The first steam accumulator used in a power station was built in Berlin, Germany in 1929 (Boardman, 2019). It was coupled to a coal-fired power station and designed to enable peak electricity output from the power station to exceed the peak capabilities of the coal boilers. A steam accumulator is essentially a pressure vessel for saturated water at high pressure. Steam is diverted from the reactor and accumulated in the vessel during storage period. Then, when steam is needed to produce power from the stored heat, a valve is open, and steam flashes out from the pressure vessel and sent to a turbine to produce power (Forsberg, 2017). Figure 12 shows a steam accumulator configuration.

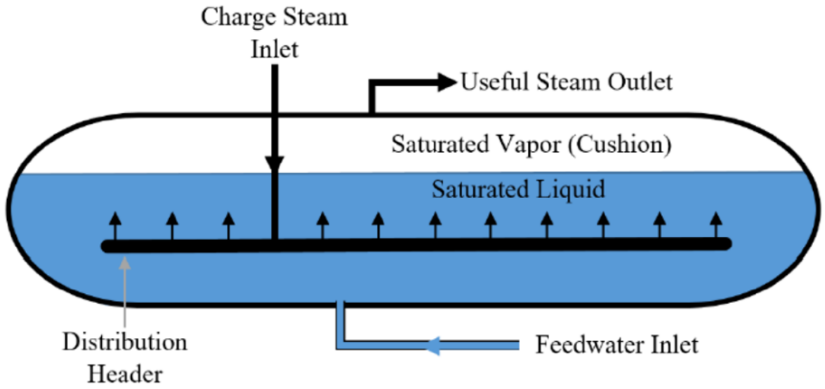

Figure 12. Steam Accumulators Configuration (Source: Boardman, 2019)

Figure 13 shows a proposed steam accumulator connected to nuclear reactors by North Carolina State University (Boardman, 2019). This configuration proposes a peaking turbine unit that is separate from the original turbine of the reactor. Steam accumulators demonstrate a potential advantage to store heat from several reactors with a separate peaking turbine which is the case of the Barakah Nuclear Power station in the UAE. Moreover, a steam accumulator storage is characterized by its very fast response. One of the major limitations of steam accumulators is that they require very expensive pressure vessels to store the high-pressure water. The high expected capital cost of heat storage can allow for daily but no longer storage times.

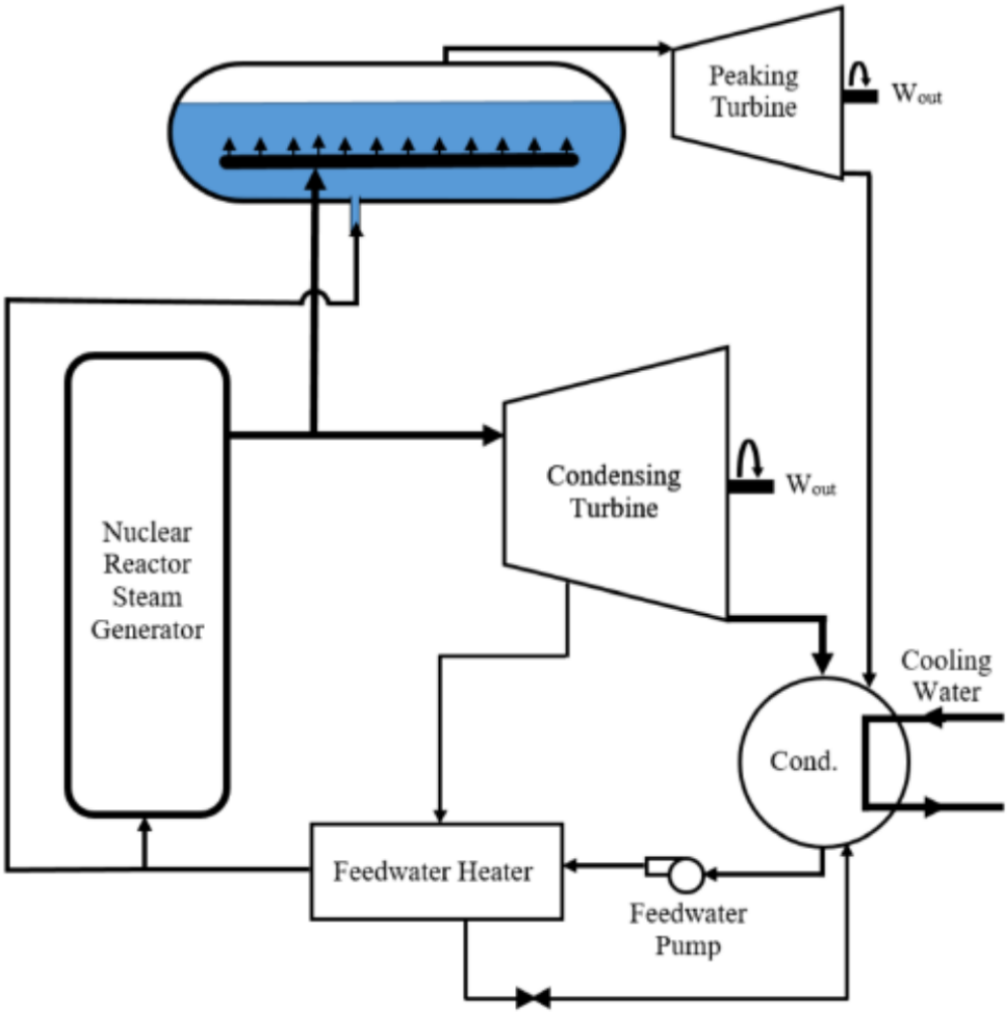

Figure 13. Steam Accumulator integrated storage system (Source: Boardman, 2019)

3.3 Geothermal Heat Storage

Geothermal heat storage is a technology that is expected to be available in the long term (Forsberg, 2017). Nevertheless, Geothermal heat storage is an attractive option to explore because it offers a heat storage option for seasonal demand variations. This demonstrates an advantage with the case of the UAE where demand for electricity fluctuates heavily between summer and winter. Air conditioning usage accounts for 57.5% of building consumption in the UAE (IRENA, 2019). During summer the demand for air conditioning is much higher than winter.

Geothermal facilities store energy by storing heat in pressurized hot water that is injected in underground. Water is passed through the reactor to heat up and then stored underground. When energy is needed, hot water is passed through a heat exchanger to extract heat and produce steam. Figure 14 demonstrates a configuration of geothermal storage unit (Forsberg, 2017).

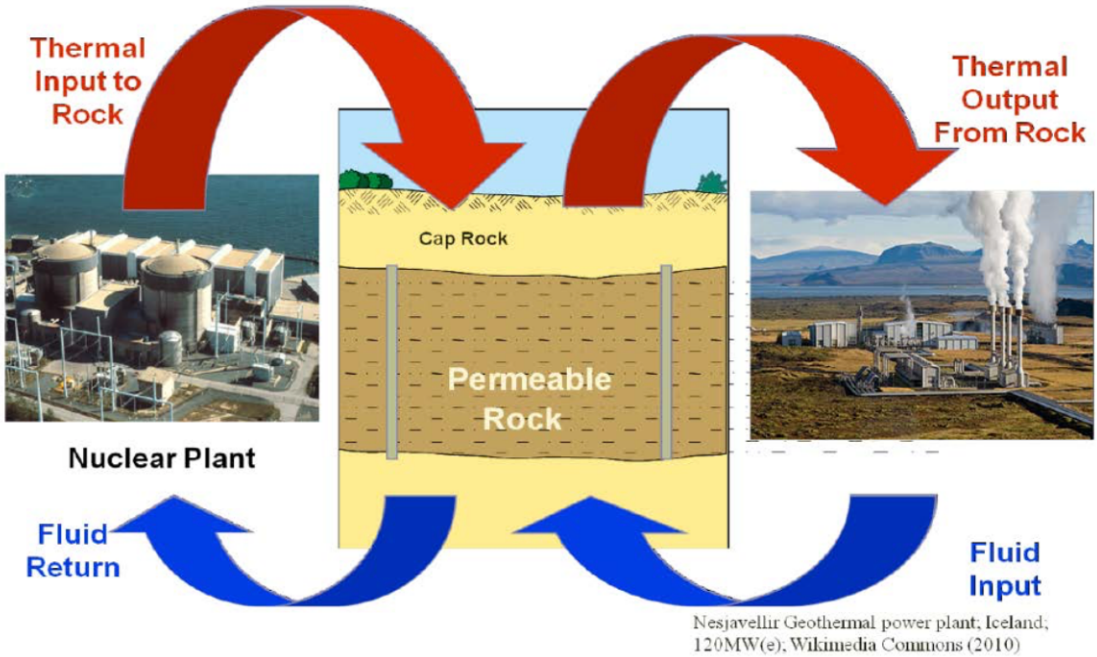

Figure 14. Geothermal storage system (Source: Forsberg 2017)

Nuclear geothermal heat storage offers higher efficiencies compared to conventional geothermal power plants for two reasons. First, nuclear geothermal storage output is much larger than conventional geothermal power plants. Second, the hot water injected in a nuclear geothermal storage is cleaner than the water injected in conventional geothermal power plants. Hot water in a traditional geothermal power plant is usually accompanied with large quantities of CO2 and other gases (Forsberg, 2017).

Geology is an important aspect that affects the applicability of geothermal storage, mainly the permeability of rock. Permeability is the ability of rock to let fluids pass through. High permeability is desirable in geothermal storage systems to reduce the pumping cost (Lee, 2010). Different types of rocks have different permeability values as seen in Figure 15. The rocks formed in the emirate of Abu Dhabi, which hosts the nuclear project in the UAE, are mostly limestone and sandstone (Irani, 2001). These two types of rocks are characterized as having high permeability. In fact, the locations rich with crude oil are usually characterized with high permeability. Therefore, location around the nuclear project in the UAE may be suitable for a geothermal storage facility. However, all geothermal options depend upon the specific local rock.

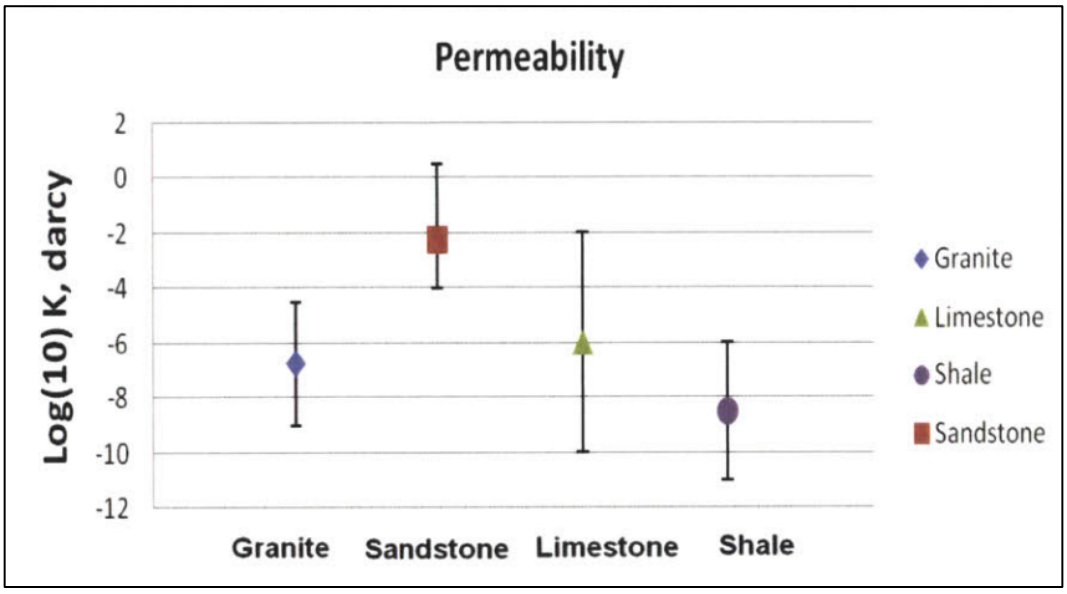

Figure 15. Permeability values for different types of rock (Source: Lee 2010)

4. Heat Storage Economic Modeling

4.1 GenX Model and Inputs

GenX is an optimization tool, or a capacity expansion modeling tool, that optimizes the energy mix of a certain region in a certain time in the future based on the target carbon emissions limit and the cost of each technology. Each case in GenX is characterized by the CO_2 emissions limit, the hourly demand profile, and the hourly availability of renewable resources. CO_2 emissions is assumed at every run while the hourly demand and availability profiles are extracted from credible sources (Jenkins & Sepulveda, 2017).

Modeling crushed rock storage coupled to Light Water Reactors using GenX has been performed in previous work (McLauchlan, 2018). McLauchalan illustrated the mechanism of using GenX for modeling heat storage with nuclear plants as seen in Figure 16. In his work, he compared the economic feasibility of investing in nuclear against nuclear with heat storage. The results from the study, applied for the Texas Grid Market, ERCOT, show that nuclear with heat storage is favorable with respect to stand-alone nuclear reactors up to a capital cost of storage of $50/kWh of heat. The analysis also showed that the benefit of using heat storage with nuclear increases with higher CO_2 emissions constraints.

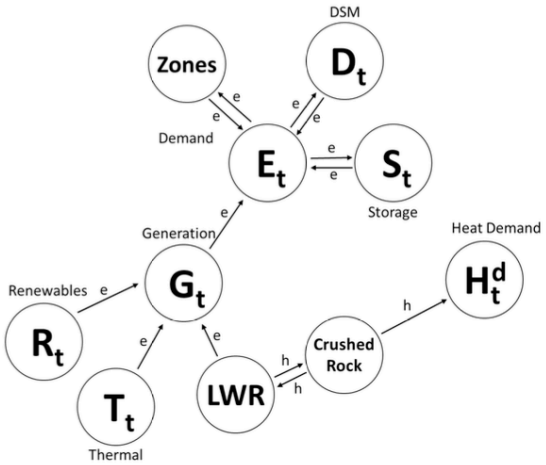

Figure 16. GenX System Level illustration of Nuclear with Heat Storage (McLauchlan, 2018)

For the purpose of the analysis of the UAE energy system, the model is developed to allow for heat storage to be added to already built nuclear reactors instead of being built together. GenX optimizes the energy mix based on a set of pre identified technology options. In the case of the UAE the existing capacities comprise of Combined Cycle Gas Turbine (CCGT), Open Cycle Gas Turbine (OCGT), Solar PV, and Nuclear. The option for adding new capacity is limited to Solar PV and Gas Turbines. This is assuming that there are no plans to build more nuclear energy than the already built, which accounts for 25% of the electricity demand. Each technology option is characterized by a set of input parameters such as the fixed and variable costs, fuel cost, and ramp up rates. Table 1 summarizes the key inputs used in the UAE GenX model. For the demand profile, the hottest day with the highest demand in the 2030 forecasted scenario of Abu Dhabi is used. The solar energy availability is obtained from renewable ninja which is an online source (Pfenninger et al., 2016). For the fuel cost and capital cost, the data is obtained from *The Future of Nuclear Energy in a Carbon-Constrained World* study for the Texas Grid market, ERCOT (MIT, 2018). It is extremely difficult to obtain technologies costs for the UAE as most numbers are classified. Therefore, the Texas market was taken as a comparable market with similar fuel prices.

Table 1. GenX Inputs

	Investment Cost ($/MW-yr)	Fixed O&M Cost ($/MWe-yr)	Variable O&M Cost ($/MWhe)	Fuel Cost ($/MMBtu)
Solar PV	$58,386	$17,000	$0.00	n/a
CCGT	$125,899	$15,800	$3.37	$7.52
OCGT	$114,334	$7,300	$10.69	$7.52
Nuclear	$455,850	$95,000	$6.89	$1.02

4.2 GenX Model Results

GenX optimizes the energy mix based on meeting the demand profile, the CO_2 emissions target, and minimizing cost, in that order of priority. The results of the analysis are presented to show the potential saving in terms of new installed Solar PV capacity to achieve CO_2 reduction goals. This is done by modeling the energy mix of the UAE in the future with and without storage coupled to the already built nuclear plants. Since the only option for capacity expansion are solar PV and CCGT, the two cases results will show how much solar PV is needed to achieve CO_2 reduction goals as well as how much gas turbines are retired. This allows for identifying the benefits of deploying nuclear heat storage regardless of prices and costs of energy sources.

The analysis is performed for two situations to compare. One without heat storage coupled to nuclear energy. The second is with heat storage coupled to nuclear energy. The storage mechanism follows the sensible heat storage discussed in section 3 of the thesis. The storage charges for 8 hours during daytime when solar availability is highest. The discharge time is for the 16 hours with lowest solar availability. The controlled parameter for the GenX testing cases is the CO_2 emissions limit. So, for both heat storage and no heat storage situations, several CO_2 limits are tested to see the effect on the final capacity installed. The CO_2 emissions in Abu Dhabi in 2017 were 420 g/kWh (Environment Agency, 2017). Assuming that the goal is to reduce CO_2 emissions by more than 50% in 2030, the target CO_2 emissions limit range considered is 160 to 180 g/kWh. The analysis finds the most economic solution given the policy constraint of allowable carbon dioxide emissions per unit of electricity producted.

Table 2 shows the detailed optimized capacities for the cases of heat storage and no heat storage for 180 g/kWh target. Table 3 shows the solar capacity savings from using nuclear heat storage for different CO_2 emissions targets. It can be noticed from the results that the solar capacity installed needed to achieve the CO_2 emissions target are reduced for the cases that utilize nuclear

heat storage. Furthermore, using heat storage allows for more gas turbine retirement. Both these effects contribute towards reducing carbon emission at lower cost compared to achieving that without nuclear heat storage.

In addition to investigating the benefit of coupling heat storage to the current fleet of nuclear reactors in the UAE, a distinct GenX case is performed to assess the benefits of expanding the generation capacity from nuclear energy in the UAE with and without heat storage. Table 4 shows the results comparing four cases at 160 g/kWh CO_2 emissions target. Two cases allowing nuclear expansion and two cases not allowing nuclear expansion. The parameters compared include solar PV installed capacity, gas turbines retired capacity, and the average cost of generation as a comparative parameter.

Table 2. GenX results for 180 g/kWh emissions

Without Heat Storage – (GW)				
Resource	Initial Capacity	Retired Capacity	New Capacity	Final Capacity
Solar PV	0.981	0	22.86	23.84
CCGT	15.254	0.52	0	14.72
OCGT	0.604	0.48	0	0.114
Nuclear	5.56	0	0	5.56
Total	22.399	1.018	22.86	44.24
With Heat Storage – (GW)				
Resource	Initial Capacity	Retired Capacity	New Capacity	Final Capacity
Solar PV	0.981	0	20.36	21.34
CCGT	15.254	1.014	0	14.24
OCGT	0.604	0.604	0	0
Nuclear	5.56	0	0	5.56
Total	22.999	1.618	20.36	41.74

Table 3. Solar PV capacity savings

CO_2 Emissions (g/kWh)	Solar PV Capacity Installed (GW)		
	w/o Storage	w/ Storage	Difference
180	22.86	20.36	2.49
170	29.48	26.92	2.56
160	37.67	33.23	4.44

Table 4. Generation capacity and average cost for 160 g/kWh emissions target cases

Case		Nuclear Installed (GW)	Solar PV Installed (GW)	Gas Turbines Retired (GW)	Average Cost of Generation ($/MW-yr)
No Nuclear Expansion	w/o Storage	-	37.67	1.01	7854.12
	w/ Storage	-	33.23	1.62	7516.29
Nuclear Expansion	w/o Storage	1.72	18.61	4.86	7239.34
	w/ Storage	1.21	21.78	5.05	7172.60

5. Low-Cost Crushed Rock Storage Design

GenX economic modeling shows that there is economic value from coupling heat storage to nuclear reactors in the UAE. In a future with large-scale renewables, variable dispatch of nuclear heat provides an alternative clean source of peak power generation. Using variable nuclear dispatch for peak power allows for more gas turbines retirement, less required solar installment and fewer batteries or other electrical storage systems to reach the target CO_2 emissions. This ideal situation for using nuclear heat storage in the UAE requires a low-cost large-scale heat storage system.

The U.S. Energy Information Agency has estimated the levelized cost of electricity for solar ($31.30/MWh) and the levelized cost of storage batteries at $121.86/MWh. While solar is inexpensive, storing that electricity for use when the sun is not shining is very expensive. The battery storage costs assume daily storage cycles. The costs are much higher if require multiday storage such as to address differences in electricity demand between weekdays and weekends. The National Renewable Energy Laboratory estimates the capital cost of storage batteries by 2030 to range from $124/kWh to $338/kWh (Cole & Frazier, 2019).

Nuclear reactors produce heat that couples to low-cost heat storage. Low-cost heat storage is desired to be able to replace expensive electricity storage associated with matching solar output to demand. The target capital cost of nuclear heat storage is in the range of $2-4/kWh. The capacity of the storage system is required to be in the range of 10-20 GWh scale in the case of daily storage and 100 GWh scale for multi-day (i.e., weekdays-weekend) storage.

Today commercial large-scale heat storage systems associated with CSP facilities use heat transfer oils or nitrate salts with hot and cold oil or salt stored in large tanks. Second generation heat storage systems that are under development add low-cost crushed rock for heat storage to

reduce capital costs. Work is underway to develop single-tank storage systems using crushed rock and nitrate salt. The tank is filled with crushed rock with hot lower-density salt on top of cold higher-density salt (Odenthal et al., 2019). The single tank design lowers tank costs and the crushed rock reduces the inventories of nitrate salts. In parallel, work is underway to develop heat storage systems using crushed rock and heat transfer oils (Amuda & Field, 2019). In these systems there are tanks of crushed rock where heat transfer oils fill the void spaces between the crushed rock in tanks only when heat is being moved into or out of storage to minimize inventories and costs of the heat transfer oil.

Designing a low-cost large heat storage requires the use of a cheap storage medium as well as maximizing the surface to volume ratio to reduce tank/building and insulation cost. The cheapest storage medium is crushed rock. Current crushed rock storage systems designed for use with Concentrated Solar Plants (CSP) include Two-tank systems and thermocline storage systems. The cost of two-tank molten salt storage systems is around $30/kWh. The use of single tank with filler material in a thermocline storage system reduces the cost of storage. A study by the Electric Power Research Institute (EPRI) shows that the cost of thermocline storage is 24% less than traditional two-tank systems. The main cost advantage is using filler material (i.e., crushed rock) instead of filling the tank with molten salt (Libby et al., 2010). The same study shows that for large thermocline storage systems (1000-3500 MWh), the cost of the storage tanks accounts for up to 40% of the total cost of the storage system.

5.1 Low-cost Crushed Rock Storage System Description

This thesis describes a third-generation heat-storage system - the Crushed Rock Ultra-large Stored Heat (CRUSH) system. In existing nitrate salt and oil heat storage systems the expensive components are the insulated tanks and the salt or other heat transfer fluid (Libby et al., 2010). The

CRUSH system as shown in Figure 17 is designed to minimize those costs. Sensible heat is stored in crushed rock piles 20 meters deep with horizontal dimensions of 250 meters by 250 meters. The heat storage material is crushed rock—the lowest cost heat storage medium.

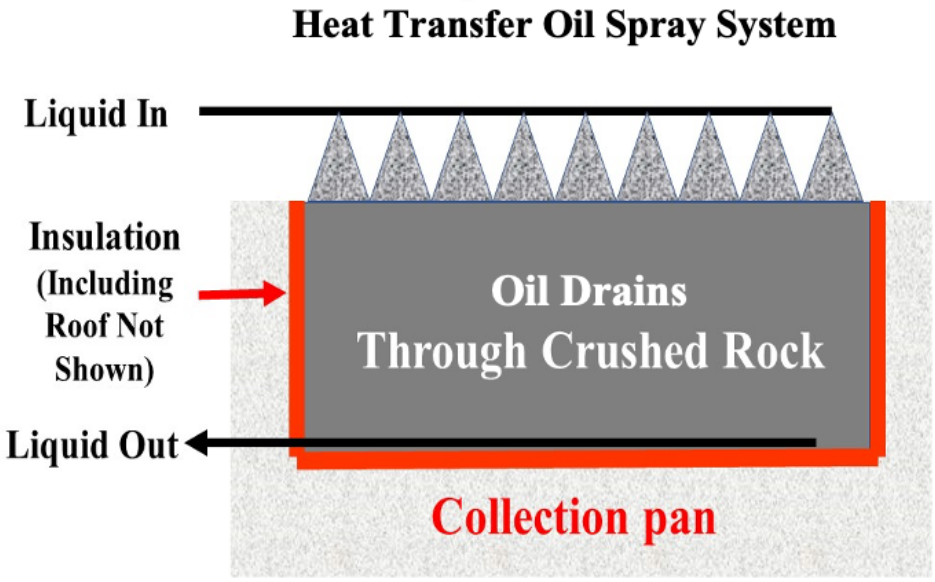

Figure 17. Cross-section or crushed-rock heat-storage system

Heat is added to the crushed rock by spraying the hot heat-transfer fluid from the nuclear plant, or any other process heat source, over the crushed rock section by section as shown in Figure 18. Each section is nominally 25 m by 25 m with the area depending upon the maximum design rate of heat input. Fluid flows by gravity through the crushed rock to the drain pan below that section of rock. The cold heat transfer fluid is collected in the bottom collection pans to be reheated. If the heat transfer oil is not fully cooled by the time it reaches the collection pan, the warm fluid is pumped onto the top of the next section of crushed rock to preheat the crushed rock. A wave of hot oil heats the crushed rock from left to right. The main conceptual difference with respect to tank-based heat storage systems is that here the fluid is used for heat transfer—not for storing heat.

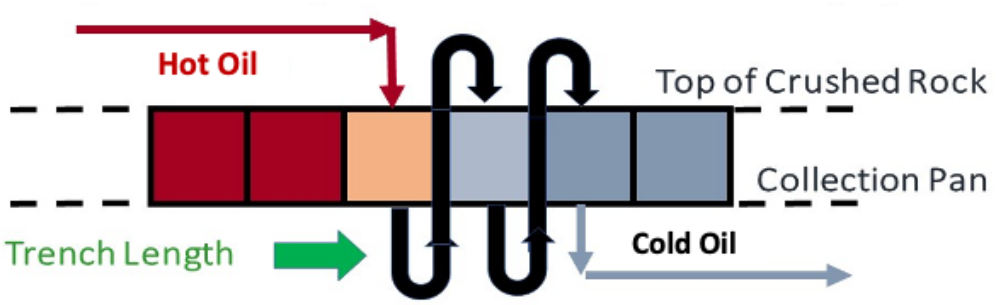

Figure 18. Side view of sequential heating of crushed rock with hot oil spray and gravity flow of liquid through the crushed rock

Heat is recovered by spraying cold heat-transfer fluid over hot crushed rock and collecting the hot oil at the bottom. There is a rock heating wave followed by a second wave to recover heat as shown in Figure 19. There are segmented collection pans under the crushed rock. When either wave reaches the end of the insulated structure, it starts over at the other end of the system. The design minimizes the inventory and cost of the heat transfer fluid that is expensive relative to the crushed rock. For a 100-GWh system, the crushed-rock bed is in the form of square that is about 250 meters on a side. If we heat a 25 by 25 meter zone at a time, the storage system would be divided into 100 zones each with its own drain pan and pumps.

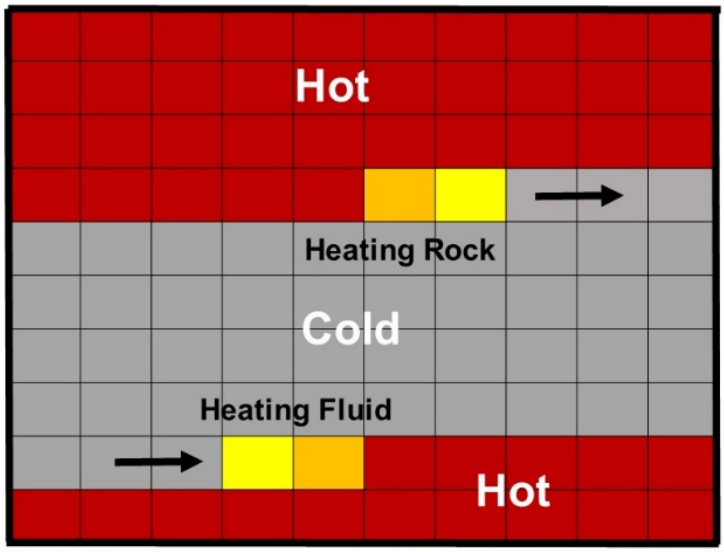

Figure 19. Top view of sequential heating and cooling of crushed rock

Figure 20 shows in more detail the sequential heating of two segments of adjacent crushed rock. Figure 21 shows in more detail heat recovery from the hot crushed rock. In the real system the crushed rock zone is 20 meters high, and the width of each segment may be 25 meters; that is, the figures are not to scale. The scale and use of gravity-drain oil for heat transfer minimizes heat transfer between adjacent hot and cold rock zones when there is no flowing fluid. It also minimizes heat transfer from the surface of the crushed rock to the gas atmosphere above and building structure. Crushed rock thermal conductivity is low because pieces of the crushed rock only touch at a few locations and the inert gas is a good insulator. When heat transfer oil is used, the inert gas would be low-cost nitrogen. This allows storage of hot and cold rock in the same container without insulated separators between the hot and cold rock. There is also the option of a thin layer of insulating rock on top—such as a layer of low-density low-conductivity crushed alumina. This is in contrast to heat storage systems with tanks of oil or liquid salts filled with crushed rock to reduce the inventory of expensive oil. In those systems natural circulation of liquid oil results in a rock pile with efficient heat transfer from hot to cold zones, which is undesirable in this application. In contrast, gases are poor heat transfer agents.

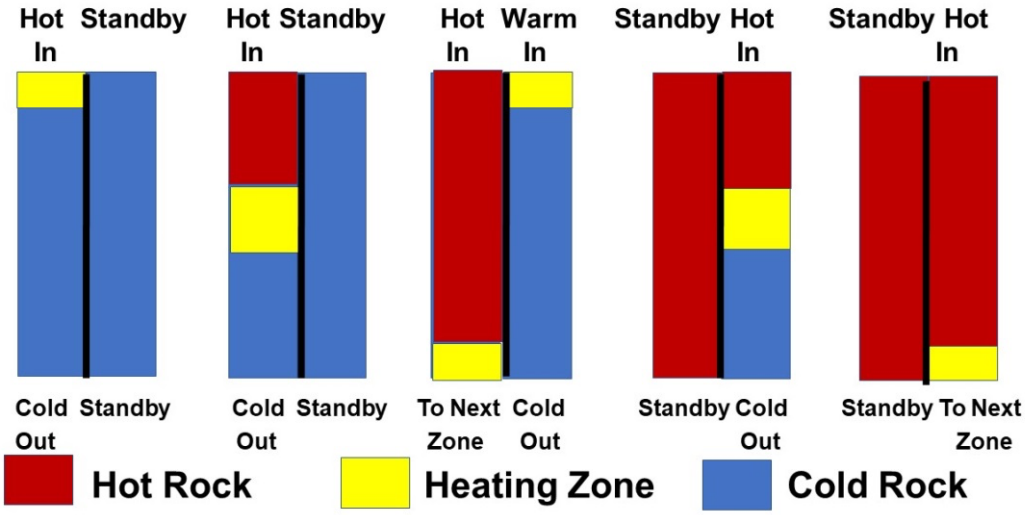

Figure 20. Sequential Heating of Two Crushed Rock Zones (Nominal height 20m and width 25m)

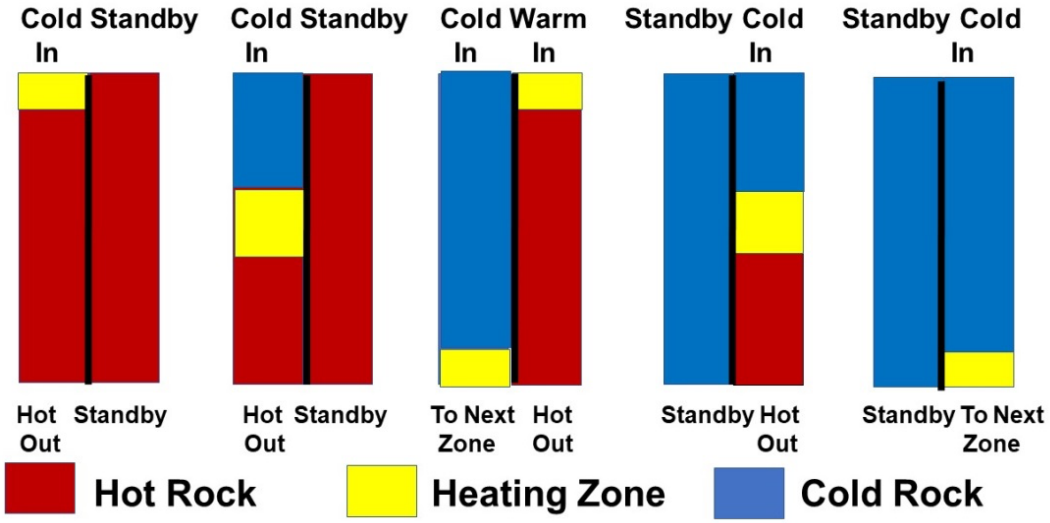

Figure 21. Sequential Heat Recovery from Two Crushed Rock Zones (Nominal height 20 m and width 25m)

This system has another safety, environmental and cost advantage relative to first- and second-generation heat-storage systems. With liquids stored in tanks, there is always a concern about leaks. The liquid imposes a hydrostatic pressure on the tank wall that provides the driving force for leaks. In this system the oil drains down to the collection pans. There is at the bottom at most a few centimeters of liquid oil on top of the sloped floor heading toward the drains. There is no large hydrostatic pressure to push liquids out of the structure if there is a leak.

The tank cost in a traditional nitrate-salt CSP system with a GWh of heat storage is almost half the total cost of the heat storage system. The capital cost of these heat storage systems is $20-30/kWh of heat storage (Libby et al., 2010). CRUSH container costs are minimized by two strategies. First, the large system minimizes the surface area (insulation and structure) per unit volume of heat capacity (crushed rock). The height is determined by experience with heap-pile leaching of copper ores. Increasing dimensions in the horizontal directions reduces container wall costs per unit of heat stored. Second, the crushed rock edges are sloped rock as shown in Figure 22. This enables free expansion and contraction of the rock with temperature and avoids the high

cost of container walls to hold in the crushed rock with added forces generated by temperature cycling of the rock. The gravity drain of fluid implies there is no fluid hydrostatic pressure on the side walls—the only requirements are that the walls be gas tight and well insulated. However, the slope of the sides of the rock pile implies a large system so that only a small fraction of the pile is slope. The building side walls and ceiling in design are similar to a very-large aircraft hangar with highly insulated interior walls and ceilings and an air-tight membrane. Unlike conventional tanks, the insulation is on the inside of the building structure with the building structural components at local air temperatures. There is no need to use expensive higher-temperature steels as is required for a hot fluid storage tank—low-cost conventional building systems are used. There is the option of curtains to reduce circulating air flow in the building structure.

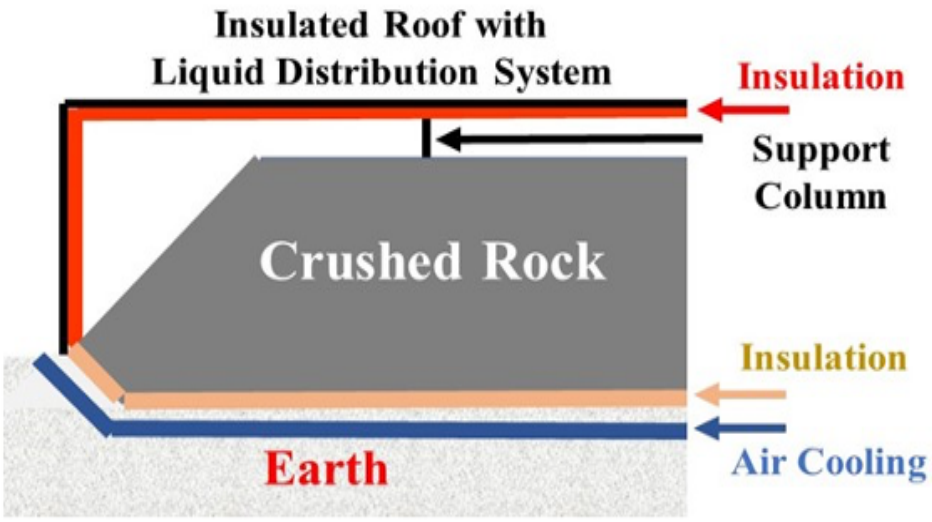

Figure 22. CRUSH sloped edges

A separate challenge is the insulated foundation structure that includes drain pans. Wan et al. has reviewed the experience with existing systems and assessed structural challenges and heat losses (Wan et al., 2020). The traditional foundation structure for two-tank heat storage is shown in Figure 23 on the left. In a two-tank system there is a hot and cold tank—neither of which sees large changes in temperature after initial startup. The fluid is in a steel tank both to contain the

fluid and provide a clean container for the fluid. The bottom of the foundation is cooled by natural circulation of air to prevent structural damage of the foundation. Addressing thermal expansion and contraction has been a major design challenge.

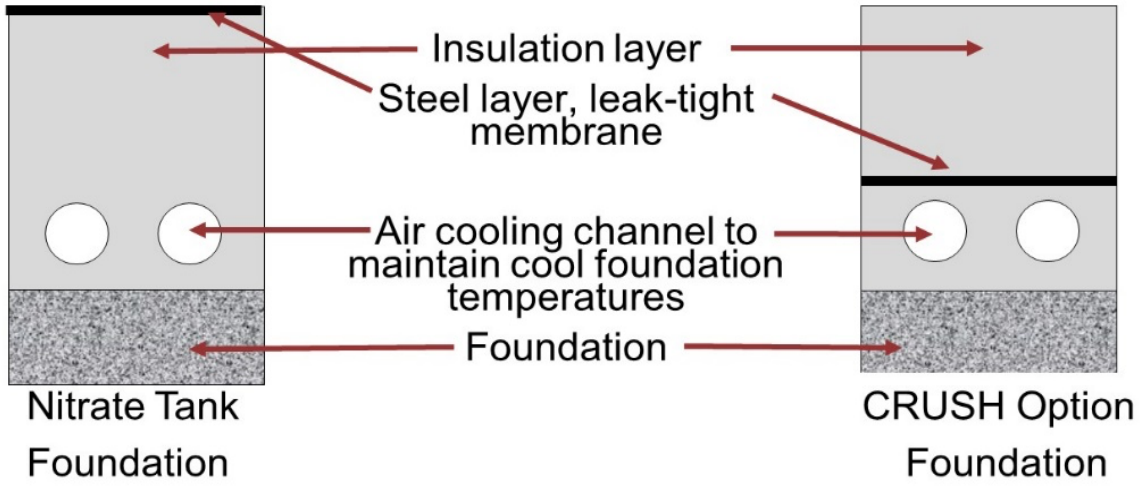

Figure 23. CRUSH Foundation Options

In the CRUSH system, the foundation sees multiple cycles of hot and cold oil. One option to address this is shown in Figure 23 on the right. The foundation and steel membrane are kept near room temperature by air-cooling channels. The insulation is between the steel membrane and the crushed rock that is heated and cooled with oil. The insulation may have multiple layers including insulating firebrick or a mixture of low-conductivity sand and other components. The liquid flows across the top of the insulation to the drains. There may be a few centimeters of residual oil depending upon drain elevation. There will be some infiltration of oil into the insulation. The thermal expansion and contraction stresses are in the insulation—not the steel container. This assures foundation integrity.

Thermal expansion and contraction of the rock will generate fines; thus, the liquid systems require on-line filters to remove these fines. Such on-line filters are used today to remove particles from crude oil. This is also why it is acceptable for the bottom insulation to be a mixture of different size particles from the size of fine sand to gravel with low thermal conductivities. If some particles

from the insulation layer are picked up by the flowing fluid, the same on-line filters that remove rock fines will remove these fines. In contrast, with traditional heat storage systems with clean oil, a steel containment is wanted to keep the heat-transfer fluid clean. However, that results in a much more complicated foundation structure to prevent damage to the steel liner during temperature transients.

CRUSH requires an off-gas system. The heat-transfer oil system will have a nitrogen atmosphere to minimize oil degradation. The building is at atmospheric pressure; thus, an off-gas system is required to avoid local air pollution as atmospheric air pressure changes and the container breaths in and out. There is the option to use commercial atmospheric breather bag systems with no gas exchange with outside air. These are large bags that inflate or deflate to adjust to the gas volume in the building.

5.2 Experience with Heap Leaching

CRUSH system has many similarities to heap-pile leaching of low-grade copper ores that is responsible for about 20% of global copper production (Bouffard and West-Sells, 2009). In heap-pile leaching a leach solution is sprayed over low-grade copper ore, drains through the pile by gravity and is collected by drain pans below the pile (Staden, 2019). Studying the experience of the heap leaching industry can provide a route for CRUSH to evolve from conceptual design to experimental work and eventually industrial scale deployment.

Heap pile leaching for copper ores can be traced back to the 1960s (Ghorbani et al., 2016). Older designs of heaps were constructed for up to 100 m in height. However, newer heaps are typically at the range of 2 to 10 m tall as it was found that the efficiency of extraction increases at smaller heights (Staden, 2019). Some heaps are constructed up to 20 m of height when insulation is of an importance (Ghorbani et al., 2016). Heap pile leaching rates are temperature sensitive and

in some cases oxygen is needed. Small pile height implies cold rock in cold weather that slows leach rates. Some ores require oxygen to enable chemical reactions. As a consequence, there is no standard height, it depends upon the local ore and local climate. Heaps are constructed to cover areas between a square kilometer and half a square kilometer, and the typical ore size is 20 or 25 mm (Ilankoon, 2012).

In heap pile leaching experiments with copper ore, experiments are used at scale to measure flow characteristics. “Columns” are used for experiments to assess the hydrodynamic performance of the heap pile. A column of packed bed is usually less than 1 m of height and close to 0.4 m in diameter. Larger scale experiments are performed using “Cribs” which are up to 7 m in height and around 2 m x 2 m in cross section. Lastly some industrial scale heaps are constructed for pilot scale experiments (Staden, 2019).

Ilankoon (2012) reported experimental results for heap pile leaching packed beds with deionized water at room temperature as the liquid. Two major characteristics of the flow were investigated: liquid holdup and hydrodynamic dispersion. Liquid holdup determines liquid residence time and wetting efficiency while hydrodynamic dispersion is caused by the uneven liquid distribution and the interconnection between the flow channels (Ilankoon, 2012). The packed bed cylindrical column used for the experiment is 243 mm wide and 800 mm tall. The particle size was varied between 0.2 to 1.8 cm. Copper ore and glass beads are used as sample particles. The fluid flow rate is varied between 1.26 to 20.16 L/h corresponding to velocities between 0.0075 mm/s to 0.12 mm/s. Heap pile leaching is partly controlled be the rate of chemical reactions and dissolution processes. One wants a solution with a high concentration of copper exiting the pile. As a consequence, high liquid flow rates are undesirable. Because the rates of heat

transfer are different than the rates of chemical kinetics, liquid flow rates per unit area in the CRUSH system may be significantly higher

To carry the experiment, steady state flow is established, and a soluble tracer is injected into the fluid. Measuring the conductivity of the tracer at the column outlet allows the investigation of the Residence Time Distribution (RTD) which is used to determine the hydrodynamic dispersion coefficient. Also, the weight of the fluid coming out of the column is measured. The weight of the liquid leaving with time shows how long for the liquid stuck in the pours to leave the system which can be converted into liquid holdup measurement. Figure 24 shows a sample of the liquid holdup and hydrodynamic dispersion results (Ilankoon, 2012).

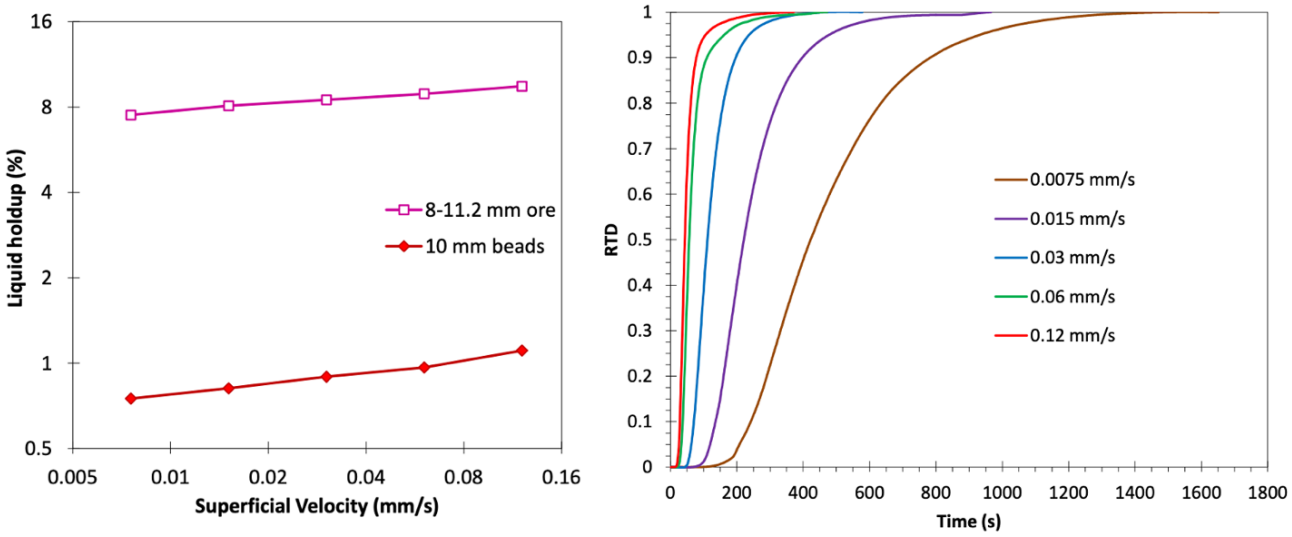

Figure 24. On the left, liquid holdup results for copper ores and glass beads. On the right, RTD measurements for glass beads (Ilankoon, 2012)

5.3 Experience with Oil CSP Systems

The use of oil in Concentrated Solar Power (CSP) systems provides much of the required technology for an oil-based heat storage from hot oil exiting storage through the steam plant and electricity production. We review herein the current state of CSP systems that use thermal oil.

There are four types of CSP systems as seen in Figure 25. They differ in the way each technology collects heat from the sun. However, the four types use some type of heat transfer fluid (HTF) to transport the heat directly to a steam turbine in the case of water as HTF or to a steam generator otherwise. Data collected in 2017 (Pelay et al., 2017) show that there are 133 CSP plants in operation. Parabolic Trough Collector (PTC) is the most used technology accounting for 65% of the operational CSP units.

PTC technology collects solar heat through a solar field of parabolic shaped mirrors focusing the light to a focal point along the parabolic mirrors line. Along the focal point, a pipe containing heat transfer fluid (HTF) absorbs the heat and heats the HTF. Thermal oil accounts for 85% of HTF used in PTC plants. Thermal oil, typically, enters the absorber tube at 293°C and exits at 393°C (Chaanaoui et al., 2016). Therminol VP-1 by Eastman and Dowtherm A by Dow are the most commonly used synthetic oils in CSP plants. They are both composed of eutectic mixture of diphenyl-oxide (DPO)/biphenyl. They are characterized by low viscosities as well as good heat transfer properties in both liquid and vapor phases. They can be used up to 400°C. The freezing temperature of Therminol VP-1 and Dowtherm A is 12°C while the boiling point is 257°C (Eastman, 2021). Therminol-66 is another candidate thermal oil for use in thermal oil systems. Therminol-66 maintains a liquid phase for the operation temperature range because of its high boiling point, 359°C, and its low freezing point, -3°C (Eastman, 2021). Peak temperatures in an LWR are near 300°C, thus, the peak oil temperatures are significantly below the oil boiling point. The low freezing point is important to avoid viscous oil at lower temperatures and avoid risk of freezing in pipes when the system is shut down. This is the leading candidate for the proposed crushed rock system because the crushed rock is operated at atmospheric pressure whereas CSP plants have the choice to operate the oil at higher pressures to maintain a liquid state if desired.

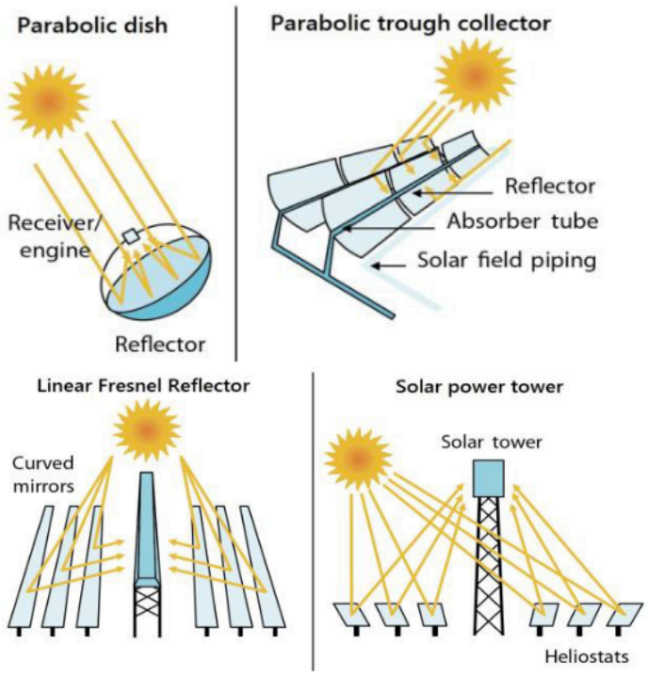

Figure 25. CSP Technologies (Chaanaoui et al., 2016)

PTC plants consist of solar fields and a power block. The solar field is where the oil is heated while the power block is where the electricity is generated using a Rankine cycle. Data collected (Pelay et al., 2017) on operational CSP units show that the capacity of oil-based PTC units ranges from 5MW to 280MW with most units rated around 50MW. The hot oil outlet temperature ranges from 348°C to 395°C with most units operating at 393°C. The efficiency of PTC units varies depending on the components of the power cycle and weather the unit is coupled to a natural gas burner. The cycle efficiency of Shams 1 in Abu Dhabi increased from 33% to 39% by superheating the steam using gas burners (Solar Thermal Energy News, 2015).

There will be some differences in the steam plant for heat storage associated with the nuclear plant relative to a solar thermal plant that will increase the heat-to-electricity efficiency for a given hot-oil temperature.

- Lower heat rejection temperatures. Most solar thermal plants are located in extremely hot climates resulting in high steam condensation temperatures that lowers plant efficiency.

The same penalty applies to nuclear plants in the same locations but will not apply to nuclear plants in other locations.

- System size. The peaking turbine coupled with nuclear heat storage will typically be larger with some gains in efficiency because larger equipment is more efficient.
- Optimized for higher efficiency. There are design tradeoffs within the steam plant where larger feedwater and condenser heat exchangers improve plant efficiency but increase capital costs. A peaking turbine coupled to a nuclear plant will operate more hours per year pushing the economics to favor more efficient design. First, significant solar plant output is near 8 hours per day with limited input in early morning or evening. That implies the nuclear heat storage system output will be near 16 hours per day with twice the capacity factor. Second, peak power from heat storage associated with a nuclear plant would be expected to operate most days of the year because nuclear plants are not impacted by cloud cover or seasonal variations.

5.4 Plant System Design

Figure 26 shows a schematic of a stand-alone heat storage cycle coupled to an LWR. There are benefits to using a stand-alone steam cycle instead of recovering the heat through the main power plant turbine. A separate steam cycle (1) allows the use of heat extracted from multiple adjacent units with one peaking turbine designed to scale, (2) reduces the licensing work with limited changes in the existing plant since the only change to the NPP is the steam extracted and the associated condensate return, (3) can be used with any steam-generating power plant with the possibility of using the same heat storage unit for multiple different steam-generating plants, (4) and enables sizing the peak generating capacity to match local market needs.

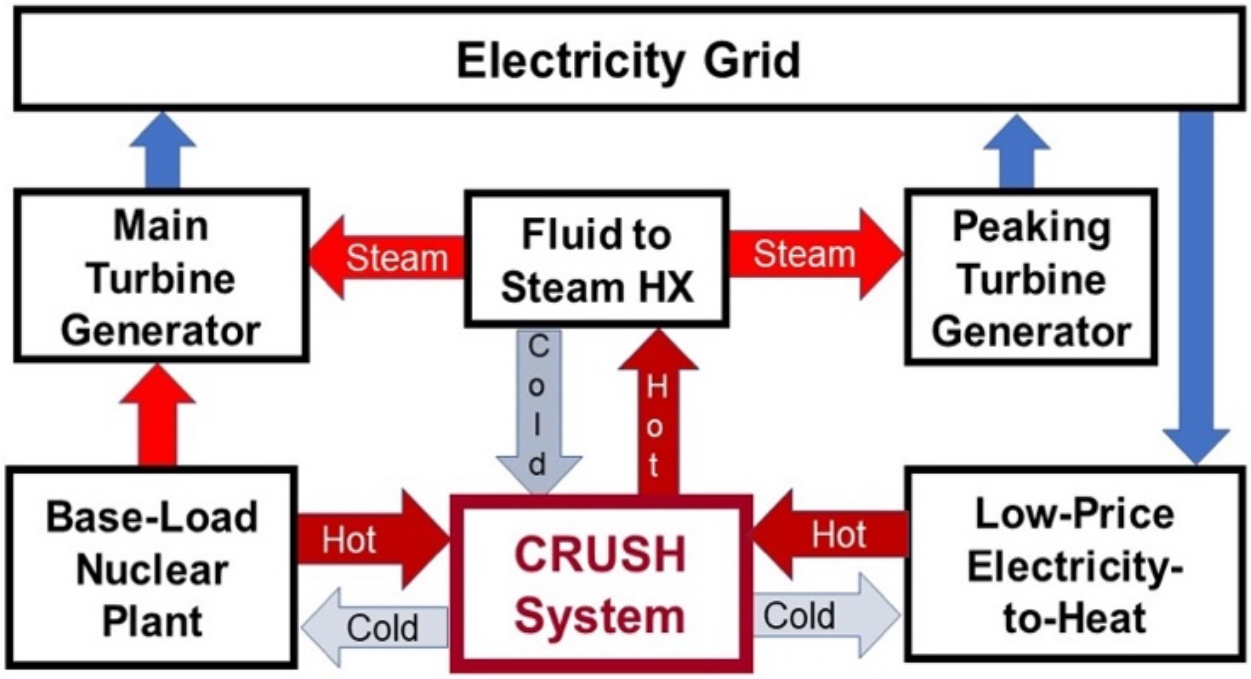

Figure 26. System Design for Heat Storage Coupled to Light-Water Reactor

As seen in Figure 26, heat is extracted from the NPP through the main steam before going to the high-pressure turbine. Heat transport medium, synthetic oil, is heated in heat exchangers (oil heaters) using the extracted steam. The hot oil is then transported to and sprayed above a trench filled with crushed rock. Heat recovery is achieved by reheating the synthetic oil by spraying cold oil over hot rock and transporting it to the stand-alone steam cycle. The rate of heat extraction is limited by the NPP secondary cycle limitations—the minimum turbine generator output for stable operation. At all times the reactor is operating at full capacity. The heat recovery rate from storage is not limited by the NPP secondary cycle. Instead, the recovery cycle is dependent on the system components of the stand-alone steam plant.

Carlson and Davidson (2021) from the University of Minnesota performed a parametric study on the thermodynamic options for a heat storage coupled to a nuclear reactor; they used AP1000 as a case study. They assessed three options for coupling nuclear energy to heat storage

as shown in Figure 27. Configuration I store heat from the high-pressure steam supply from the steam generator and discharges the heat to the low-pressure turbine. Configuration II also charges from the high-pressure steam supply but discharges a preheated condensed feedwater to the steam generator. Configuration III stores heat from the low-pressure steam supply and discharges heat in a stand-alone steam cycle. Configuration III stores heat from low-pressure steam supply because as a previous study (Carlson & Davidson, 2020) showed that the capacity factor of the overall system is higher when heat is extracted from the low-pressure steam supply compared to the high-pressure steam supply. The results of the analysis comparing the three configurations show that configuration III is the most favorable as it produces the highest energy production ratio and peaking power of more than 1.5 times the baseload power (Carlson & Davidson, 2021).

Kluba and Field (2019) performed an exergy analysis on the coupling of crushed rock heat storage to the APR 1400 reactor. The crushed rock storage system is the system developed by KINGS university in South Korea as described in section 3 of the thesis. The configurations they used is similar to Configurations I and II from the Carlson and Davidson study. In those two systems high-pressure steam is diverted to storage. Heat from storage is used to supply steam to the low-pressure turbine (Configuration I,) or preheat feedwater (Configuration II). They assessed the thermodynamic performance of the system for three temperature drop cases, 55°C, 85°C, and 125°C. The three temperatures correspond to three different heat recovery paths. The temperature-drop cases of 55°C and 125°C correspond to heat recovered as preheated feedwater at different locations. One before the feedwater heaters and the other after the feedwater heaters respectively. The 85°C temperature drop case correspond to the heat recovery as superheated steam before the low-pressure turbine.

There are two sources of exergy destruction in the system as described by Kluba and Field. One is the sensible and latent heat transfer between water/steam and oil. The second is the mixing of fluids at the junctions where steam is extracted/supplied. The irreversibility due to heat transfer increases as the temperature drop increases. The irreversibility due to mixing increases as the working fluid flow rate increases. The analysis concluded that the 125°C case is preferable with an estimated roundtrip efficiency more than 80% (Kluba & Fields, 2019). Table 5 shows the thermodynamic parameters for the three cases. The roundtrip efficiency is the ratio of the power generated during discharge compared to the power that could have been generated with baseload. The peak power is the relative maximum power during discharge compared to the baseload power.

In some types of CSP plants, heat transfer oil goes thorough the solar collector, is heated and the hot oil is sent to a steam generator. The steam is then used to produce electricity. CSP technology can be used as a reference design for this peaking steam cycle. There are many components that can be implemented directly from CSP plant designs; oil heaters, fast ramp-up/down steam turbines, and oil piping are some examples. The peaking turbine of the storage unit needs to acquire specific features that allows it to be turned on and off rapidly on a daily cycle. CSP plants often are operated in a similar daily cycle following the solar irradiation patterns. Thus, CSP steam turbines are designed to be turned on and off daily. M.A.N and Siemens design these special turbines up to 250 MWe (Solar Thermal Energy News, 2015).

Table 5. Thermodynamic parameters for integrated storage steam cycle (Kluba & Field, 2019)

Case Number	Temperature Drop	Relative Peak Power	Roundtrip Efficiency
Case 1	55°C	1.139	74.8%
Case 2	85°C	1.132	70.7%
Case 3	125°C	1.132	80.1%

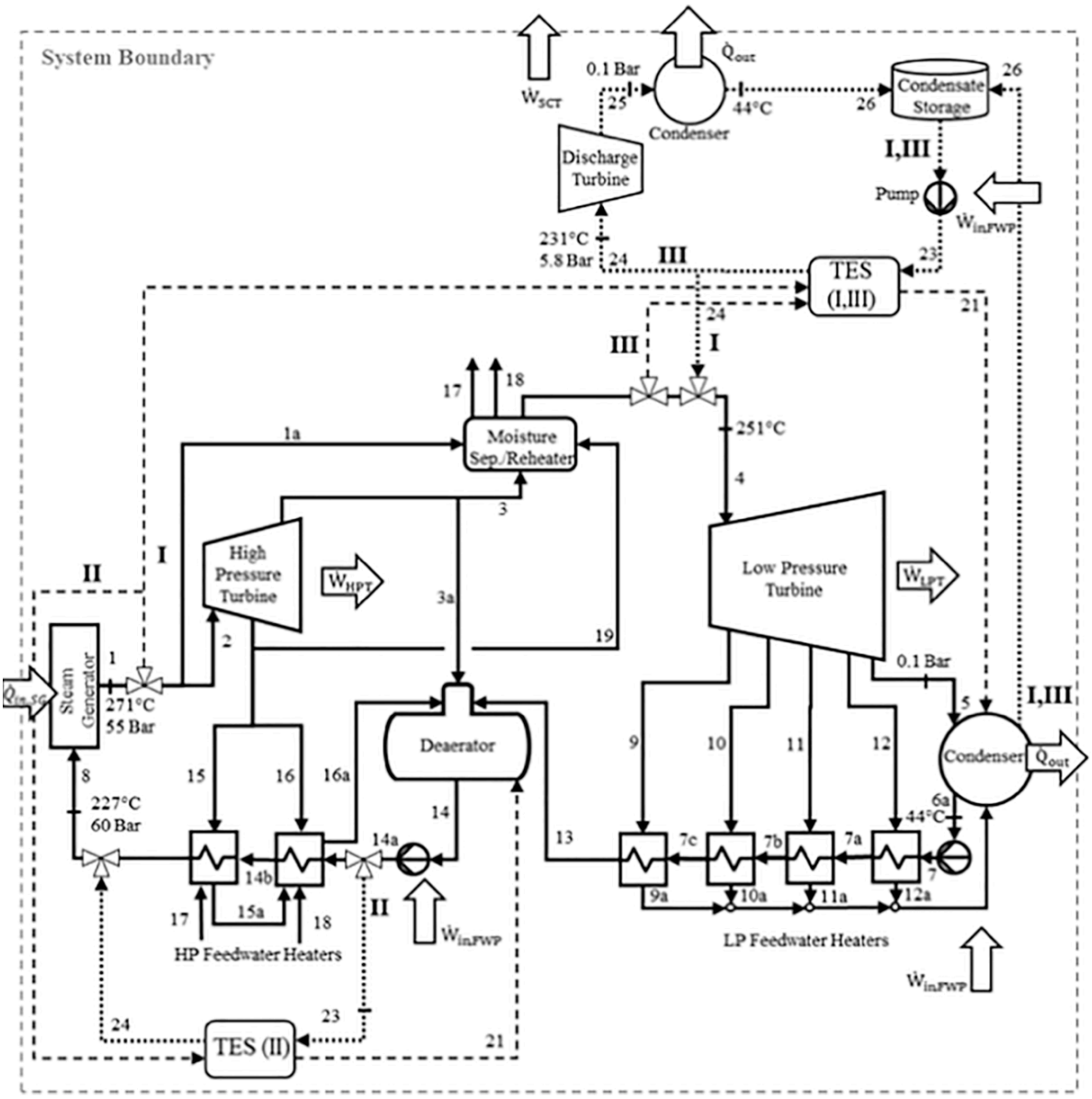

Figure 27. Heat Storage Integration to Reactor Configuration (Carlson & Davidson, 2021)

5.5 CRUSH Design Considerations

From the design perspective, the optimum crushed rock size is a major design consideration because of two reasons. First, the cost of procuring crushed rock depends on crushed rock size as more crushing work is required to reach finer sizes of rock. Second, the decision of crushed rock size has an impact on the assumptions of engineering modeling of the storage system as described in the next chapter of this thesis.

There is an optimum crushed rock size determined by a tradeoff between fluid flow and heat transfer. If we had a crushed rock bed where each piece of crushed rock was a meter in size and a hot liquid was poured on top of the bed, the liquid would flow downward to the catch pan within a few seconds. Heating of the rock would be slow because heat transfer would be limited by conduction of heat from the surface of the one-meter-diameter boulders to the center of each rock. The hot fluid would be only partly cooled by the time it reached the collection pan because there was not enough time or surface area to transfer heat to the rock.

As we reduce the rock size, several things happen. First, it takes more time for the liquid to reach the collection pans. The fluid has to flow around more pieces of rock. Gravity wants to accelerate the fluid in the downward direction, but smaller crushed rock sizes imply a longer flow path with viscous resistance to liquid flow to the collection pan. This is a water slide problem. If we have a water slide that is short and steep, water flows quickly from top to bottom. Gravity wants to accelerate water flow, but the bottom surface of the slide offers resistance to downward flow of liquid. If we have a longer water slide with a shallow slope, water takes more time to flow from top to bottom. The longer surface of the water slide slows the water. The same is happening here as the rock size is reduced.

In terms of heat transfer, as we go to smaller diameter crushed rock, the heat conduction distance from the surface to the center of each rock decreases. This accelerates heat transfer. At the same time heat transfer from fluid to rock improves because there is much more surface area.

There are other constraints. There is an upper limit to the gravity flow rate of liquid through the rock pile. As the rock sizes get smaller, the path length for liquid flow increases. The cover gas might become entrained by the downward flow, which increases liquid flow resistance. As the rock size becomes very small, surface tension holds the liquid between pieces of rock. If the

crushed rock is the size of sand particles, flow time from the top of the pile to the bottom may be measured in hours or days versus minutes. The flooding limit decreases; that is, the maximum flow rate of liquid that will flow through a square meter cross section of the crushed rock pile decreases.

Based on experience, the nominal crushed rock diameter will be measured in centimeters with the optimum diameter partly dependent upon bed height, desired fluid temperature drop and rock properties. Important rock properties include thermal conductivity, volumetric heat capacity, surface properties and geometric shapes. High-thermal conductivity implies larger rock sizes because of more rapid movement of heat from the surface to the pebble interior. High volumetric heat capacity implies smaller rock sizes because more heat is stored per unit volume of rock and more heat must be transferred from the liquid to the rock. Surface properties (smooth, rough) change liquid flow velocities around each piece of crushed rock. Rocks when crushed that produce relatively round rocks will pack differently than rocks with greater length-to-width ratios. Analysis will allow general design; but experiments are required to validate performance.

Partly decoupled from thermal hydraulic considerations is the long-term holdup of oil in the crushed rock. Residual fluid holdup is to be minimized because of the cost of the fluid versus the crushed rock. Surface tension will result in holdup of fluid at points where rocks touch each other. Smooth rock surfaces result in less residual liquid on surfaces. Fluid holdup considerations may eliminate some types of rock as fill material and create incentives for larger pebble sizes with smaller total surface area. Earlier studies (Molina et al., 2019) have identified some candidate rock types.

There is relevant experience from other industries. There has been significant work on crushed rock heated by hot air. In the mining industry, heap pile leaching is used. Low-grade ores are crushed and placed in large piles. Solutions are sprinkled on top of the pile and flow through

the pile leaching the valuable copper or other elements into the liquid and are collected by drain structures under the rock pile. The most relevant experience is heap-pile leaching.

There are a variety of trickle filters with similar geometry. Trickle filters are used to treat wastewater where biological growths on the crushed rock degrade the organics in the wastewater. Last, cooling towers with the fans turned off operate in a similar manner. These systems use highly engineered packings.

6. Heat Storage Engineering Modeling

Heat transfer of two-phase flow in packed beds is a well-established field of study. Previous work includes heat storage technologies such as single tank thermocline storage with filler material as well as heap-pile leaching. The heat transfer model determines the temperature gradient transient of the crushed rock pile. The temperature gradient transient is used to determine the sizing of the heat storage system as well as the option space for the engineering parameters such as bed height, flow rate, and crushed rock particle size.

The analysis starts with the derivation of a two-phase one-dimensional numerical model for the CRUSH system. The model is a first-generation model that uses assumptions and approximations. It is not supposed to be an accurate representation of CRUSH performance, but a tool to explore the behavior and option space of CRUSH. The second part of the analysis investigates the option space of several parameters that defines the CRUSH system. Finally, the last part explores the parameters related to the sizing of the storage system.

6.1 Nomenclature

Table 6 shows the nomenclature used in this section.

Table 6. Engineering modeling nomenclature

Latin Letters		Dimensionless Numbers	
A	Area [m^2]	Pr	Prandtl Number [-]
C	Specific Heat [J kg^{-1} K^{-1}]	Re	Reynolds Number [-]
d_p	Particle Diameter [m]		
E	Total Energy [J]	Greek Letters	
G	Mass Flux [kg m^{-2} s^{-1}]	ρ	Density [kg m^{-3}]
g	Gravitational Constant [m s^{-2}]	μ	Dynamic viscosity [Pa s]
h	Volumetric heat transfer coefficient [W m^{-3} K^{-1}]	ε	Porosity [-]
k	Thermal conductivity [W m^{-1} K^{-1}]		
L	Packed Bed Height [m]	Subscripts	
m	Mass [kg]	f	Fluid
$\dot{m}$	Mass flow rate [kg s^{-1}]	s	Solid
ΔP	Pressure Drop [Pa]	tot	Total (the whole trench)
$\dot{Q}$	Heat Rate [W]	eff	Effective
q''	Heat Flux [W m^{-2}]	in	at trench inlet
T	Temperature [K]	out	at trench outlet
t	Time [s]	dep	Deposited
v	Velocity [m s^{-1}]		
V	Volume [m^3]		
X	Axial coordinate [m]		

6.2 Heat Transfer and Fluid Flow Modeling

Modeling heat transfer and fluid flow in a crushed rock pile can be performed in either 1-D or 2-D models. The major difference is that in a 1-D model crushed rock is assumed to be a continuous medium with continuous pores for the fluid flow. Hoffmann et al. show that numerical 1-D models reasonably agree with industrial experiments' results of crushed rock pile heat transfer (Hoffmann et al., 2016). Figure 28 shows a schematic of the control volume of the crushed rock and thermal oil storage. For the purpose of this thesis a one-dimensional two-phase model is developed with the following assumptions:

1. Constant crushed rock porosity through the bed
2. Identical spherical particles for crushed rock
3. Constant mass flow rate through the bed
4. Neglect heat losses through the wall as the system is very large
5. Neglect conduction through oil due to small temperature gradient (but conduction through the rocks is included in the model)
6. Neglect radiation heat transfer
7. No inert gas entrainment, i.e., the space between rocks is occupied entirely by the fluid.

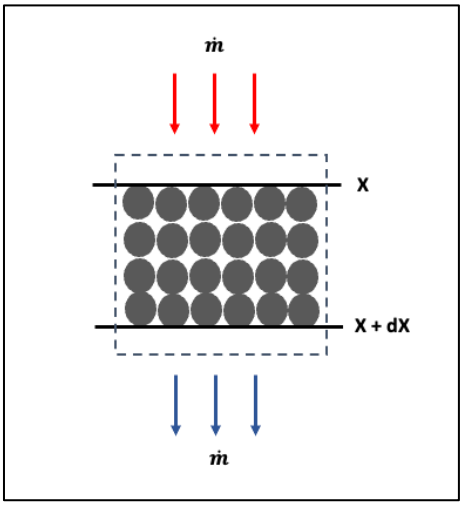

Figure 28. Crushed rock and oil heat transfer control volume

6.2.1 Model Derivation

The constitutive relations of the heat and mass transfer of the crushed rock and synthetic oil storage system are derived from the conservation of energy and mass equations of the control volume. First, mass conservation through the control volume describes the mass transfer within the control volume. The heat transfer fluid, synthetic oil, is the only substance moving in and out of the system and is denoted 'f' in the equation. The two terms on the right-hand side of the equation are the mas flow rates of the oil at inlet and outlet.

$$\frac{dm_f}{dt} = \dot{m}_X - \dot{m}_{X+dX} \qquad \textit{Eq. 1}$$

$$m_f = \rho_f A_{tot} dX \varepsilon \qquad \textit{Eq. 2}$$

$$\dot{m} = \rho_f v_f A_{tot} \varepsilon \qquad \textit{Eq. 3}$$

From equations 1, 2, and 3 it is found that v_f is constant

$$v_f = \frac{\dot{m}}{\rho_f A_{tot} \varepsilon} = \frac{G}{\rho_f \varepsilon} \qquad \textit{Eq. 4}$$

The energy conservation equation describes the balance of energy (heat and work) through the system. Energy conservation is stated for each element of the system. The storage system does not experience work transfer. The terms of the equations reduce to the heat transferred either by convection, conduction, or radiation, and the enthalpy flow in and out of the system. As stated in the assumptions, radiation and conduction through the heat transfer fluid is neglected. The energy equation of the fluid is:

$$\frac{dE_f}{dt} = \dot{Q}_f + \dot{m}_X C_{f,X} T_{f,X} - \dot{m}_{X+dX} C_{f,X+dX} T_{f,X+dX} \qquad \textit{Eq. 5}$$

$$E_f = m_f C_f T_f \qquad \textit{Eq. 6}$$

Where convection between crushed rock and oil is

$$\dot{Q}_f = -hA_{tot}dX(T_f - T_s) \qquad \textit{Eq. 7}$$

From equation 1 through 7

$$\varepsilon\rho_f C_f\left(\frac{\partial T_f}{\partial t} + v_f\frac{\partial T_f}{\partial X}\right) = h(T_s - T_f) \qquad \textit{Eq. 8}$$

The energy conservation equation for the crushed rock includes the heat convection and conduction through the rock where $q^{"}$ is the conduction heat flux through the rock

$$\frac{dE_s}{dt} = \dot{Q}_s \qquad \textit{Eq. 9}$$

$$E_s = m_s C_s T_s \qquad \textit{Eq. 10}$$

$$m_s = \rho_s A_{tot}dX(1-\varepsilon) \qquad \textit{Eq. 11}$$

$$\dot{Q}_s = hA_{tot}dX\left(T_f - T_s\right) + q^{"}_X A_{tot}(1-\varepsilon) - q^{"}_{X+dX}A_{tot}(1-\varepsilon) \qquad \textit{Eq. 12}$$

$$q^{"} = -k_{seff}\frac{\partial T_s}{\partial X} \qquad \textit{Eq. 13}$$

$$k_{seff} = (1-\varepsilon)k_s \qquad \textit{Eq. 14}$$

From equation 9 through 14

$$(1-\varepsilon)\rho_s C_s\frac{\partial T_s}{\partial t} = h\left(T_f - T_s\right) + k_{seff}\frac{\partial^2 T_s}{\partial X^2} \qquad \textit{Eq. 15}$$

Solving equations 1 through 15 requires two initial conditions for T_f and T_s, one boundary condition for T_f, and two boundary conditions for T_s. Equations 16 and 17 show the initial conditions for the solid and fluid temperatures which are known by design. Equation 18 shows the inlet boundary condition for the fluid which is dependent on the reactor extracted heat. Equations 19 and 20 show the adiabatic boundary condition of the solid and fluid.

$$T_{f,@\ t=0} = T_{fo} \quad \textit{Eq. 16}$$

$$T_{s,@\ t=0} = T_{so} \quad \textit{Eq. 17}$$

$$T_{f,@\ X=0} = T_{f,in} \quad \textit{Eq. 18}$$

$$\frac{\partial T_s}{\partial X}_{@\ X=0} = 0 \quad \textit{Eq. 19}$$

$$\frac{\partial T_s}{\partial X}_{@\ X=L} = 0 \quad \textit{Eq. 20}$$

6.2.2 Heat transfer Coefficient

Choosing the appropriate heat transfer coefficient is essential for modeling solid-fluid heat transfer. Heat transfer coefficients are developed based on various parameters such as geometry, type of flow, and boundary conditions. Xu et al. listed a number of interstitial heat transfer coefficients between fluid and solid for packed beds found in the literature (Xu et al., 2012). The following correlation is used throughout this thesis.

$$h = \frac{6(1-\varepsilon)k_{feff}[2 + 1.1Re^{0.6}Pr^{1/3}]}{d_p^2} \quad \textit{Eq. 21}$$

$$Re = \frac{\rho_f d_p v_f}{\mu_f} \quad \textit{Eq. 22}$$

$$Pr = \frac{C_f \mu_f}{k_f} \quad \textit{Eq. 23}$$

$$k_{feff} = \varepsilon k_f \quad \textit{Eq. 24}$$

6.2.3 Crushed Rock and Oil Parameters

As discussed in section 5 of the thesis, Therminol-66 is selected as the heat transfer fluid for its appropriate operating temperatures. Therminol-66 properties are listed in Table 7. Various types of crushed rock are compatible with thermal oils (Molina et al., 2019). The selection is based on the cost and availability in the region. Quartzite and Granite are used for the analysis in this thesis. The properties of Quartzite ad Granite are listed in Table 8. A common value of 0.2 is used

for the porosity (ε). This value depends upon the size distribution of crushed rock and can be as large as 0.4.

Table 7. Properties of heat transfer fluid – Therminol-66 (Eastman 2021)

ρ_f	$kg\ m^{-3}$	1225.4 - 0.7281 * T_f
C_f	$J\ kg^{-1}\ K^{-1}$	(0.483 + 0.0036 * T_f) * 1000
k_f	$W\ m^{-1}\ K^{-1}$	-2*10^{-7} * T_f^2 + 5*10^{-5} * T_f + 0.1153
μ_f	Pa s	8*10^{18} * $T_f^{(-8.147)}$

Table 8. Properties of different rock types (Hoffmann 2016)

Quartzite	ρ_s	$kg\ m^{-3}$	2500
	C_s	$J\ kg^{-1}\ K^{-1}$	830
	k_s	$W\ m^{-1}\ K^{-1}$	5.69
Granite	ρ_s	$kg\ m^{-3}$	2643
	C_s	$J\ kg^{-1}\ K^{-1}$	1020
	k_s	$W\ m^{-1}\ K^{-1}$	2.2

6.2.4 Numerical Model

Equations 1 through 24 are numerically solved by means of finite difference method. With a second order central differencing scheme for the second order derivative terms, a central differencing scheme for the first order derivative terms and an explicit scheme for the time discretization. The model (Appendix A) is solved using Python 3.9. The model is verified by comparing sample results to a one-diemnsional thermal equilibrium model solved analytically by Allen (2010) and McLauchlan (2018) as shown in Appendix A.

6.2.5 Option Space for Heat Transfer Model

Several parameters in the model are selected by the designer. This creates an option space for the designer. This thesis reports on the early development of the CRUSH system. The design space has been only partly explored; thus, the chosen values of different design parameters should be viewed preliminary—not necessarily optimum design choices. Five parameters are analyzed in this section. Crushed rock particle size, gravitational flow rate, packed bed height, the temperature differential between hot and cold, and the velocity of fluid flow through the pile.

6.2.5.1 Crushed Rock Particle Size

Assuming a continuous medium of crushed rock (1-D model) can be justified by studying the heat transfer and fluid flow dependencies on crushed rock particles size. Heat transfer modeling of a single crushed rock particle will determine the range of rock sizes where heat transfer within rock particles is much faster compared to the scale of heat transfer of the system. If the rate of heat transfer in single pieces of rock is fast relative to the system, we can assume instantaneous heat transfer and ignore this heat transfer delay in the analysis.

Internal rock heat transfer transients are modeled by using Heisler Charts for spherical geometries. Heisler Charts are used to determine the time it takes for the temperature at the center of a sphere to reach equilibrium with the environment (Cengel, 2007). In this model, a rock particle is subject to continuous heat convection from a fixed temperature environment, in this case, a heat transfer fluid. The rock particle is in room temperature while the heat transfer fluid is at 280^{o}C. The analysis is performed using the properties of Therminol-66 as heat transfer fluid and quartzite and granite as crushed rock samples. Heisler Charts represents the centerline temperature as a dimensionless temperature difference with the environment compared to the initial temperature difference up to 0.1% of the original temperature (Cengel, 2007). In other words, in the case of a

rock heating from room temperature to 280ºC, the time calculated using Heisler Charts is when the centerline temperature reaches 99.92% of the environment temperature.

Figure 29 shows the time frame of heat transfer within a rock particle for different rock sizes. It can be concluded that for crushed rock sizes up to 10-12 cm in diameter, the heat transfer within crushed rock happens much faster (minutes) compared to the scale of the system heat transfer and fluid flow from top to bottom (hours). For the purpose of the sensitivity analysis performed in the rest of this section, a value of 2 cm for the rock size is selected.

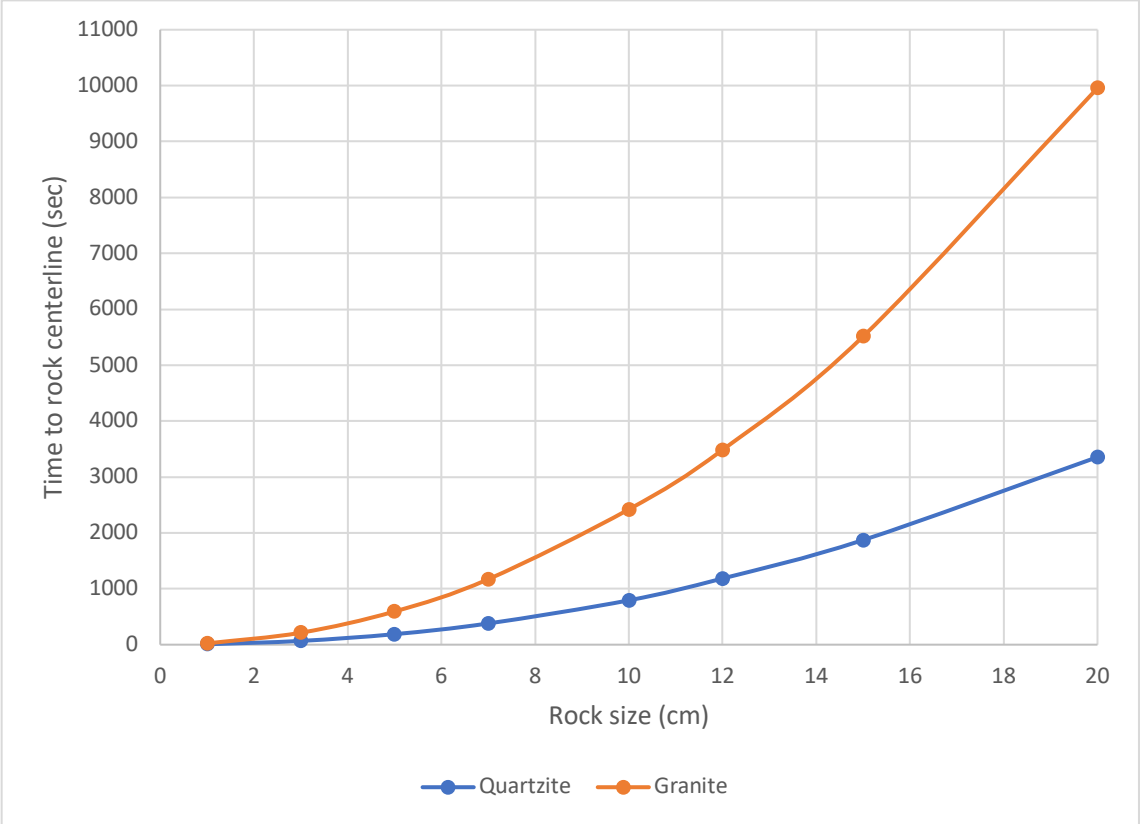

Figure 29. Time to heat up a rock particle

6.2.5.2 Gravitational Flow Rate

The total oil flow rate coming to the crushed rock storage is determined by the diverted heat from the power plant. The designer then selects a section area to pour the oil on top of. The maximum allowable mass flux of oil in the crushed rock section is governed by the gravitational flow of oil from top to bottom of the trench. The total pressure drop in the system is zero because the whole system is at atmospheric pressure. The oil flows from top to bottom through gravity only. Therefore, the mass flux should not exceed the value that will cause the friction forces to overcome the gravitational forces. This will cause flooding.

Pressure drop through the trench is modeled to analyze the gravitational and friction forces that drive the flow of oil.

$$\Delta P_{total} = \Delta P_{friction} + \Delta P_{gravity} + \Delta P_{form} + \Delta P_{acceleration} \qquad \textit{Eq. 25}$$

The acceleration term accounts for the pressure change due to change in fluid density. The form term accounts for pressure change due to inlet and outlet formation. The main terms that drive the flow of fluid in a packed beds are the friction and gravitation terms (McLauchlan 2018).

The gravitation pressure-drop depends on the density of the fluid and the height of the bed.

$$\Delta P_{gravity} = \rho_f g L \qquad \textit{Eq. 26}$$

The friction pressure drop depends on the flow type, the channel geometry, and the fluid characteristic. Several correlations were developed for packed bed fluid flow friction pressure drop. The most popular is developed by Ergun (1952) for 0<Re<3000 (Allen 2010).

$$-\frac{\Delta P_{friction}}{L} = 150\frac{(1-\varepsilon)^2}{\varepsilon^3}\frac{\mu_f v_f}{{d_p}^2} + 1.75\frac{(1-\varepsilon)}{\varepsilon^3}\frac{\rho_f {v_f}^2}{d_p} \qquad \textit{Eq. 27}$$

Figure 30 shows the maximum allowable mass flux that will allow for gravitational flow of the oil through the trench without causing flooding. The properties of Therminol-66 are used.

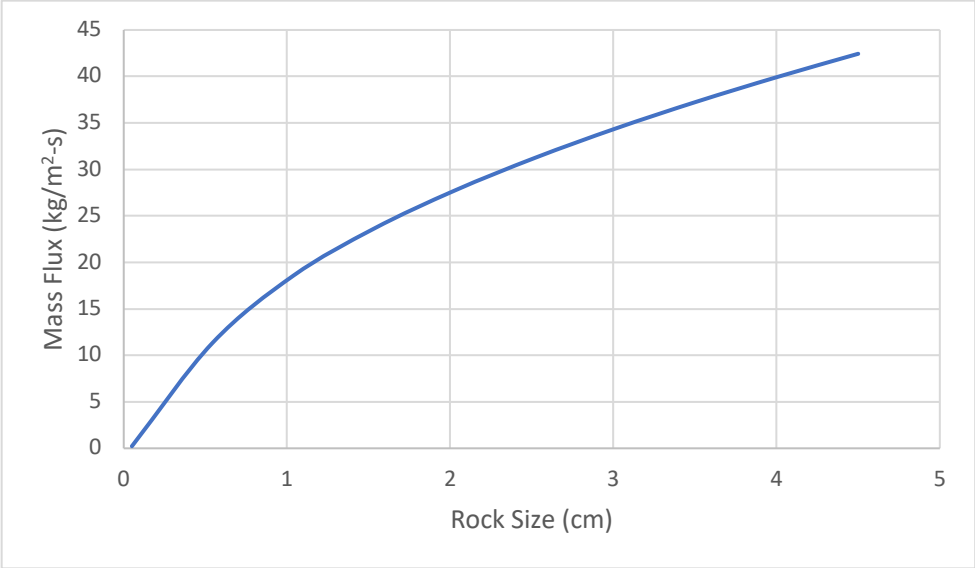

Figure 30. Maximum allowable gravitational mass flux of Therminol-66 in packed beds

6.2.5.3 Packed Bed Height

Because of the sequential heating nature of the system, the height of the packed bed does not affect the total energy stored. The height of the crushed rock is chosen based on several engineering tradeoffs.

- Rock compressive strength. The rock must maintain its integrity. If very high crushed rock piles, rock at the bottom may fail and crumble creating a blockage
- Uniform fluid flow. If there is non-uniform flow, the maximum distance that condition can exist is to the drain pan. Very high piles can have larger non-uniform distributions.
- Structural considerations associated with the building structure.
- Pumping costs from one column to the next. If the oil is not fully cooled by the time it reaches the drain pan, it is pumped onto the next section of crushed rock to be further cooled. If one had a very short crushed-rock height, the hot-cold transition zone would be much longer then the pile height. One would be forced to repeatedly pump oil from one stack of crushed rock to the next to fully cool the oil—an expensive proposition. We need

a height, so we do not pump oil more than once from one crushed rock zone to the next crushed rock zone.

Figure 31 shows the effect of the bed height and the charging time of one section of the bed. The temperature drop is assumed to be 200°C and quartzite properties are used for crushed rock. Appendix B includes the results for Granite. A value of 20 m is chosen for further analysis in this section. Many heap-leaching piles for recovery of copper and other minerals have similar heights (Ilankoon, 2012).

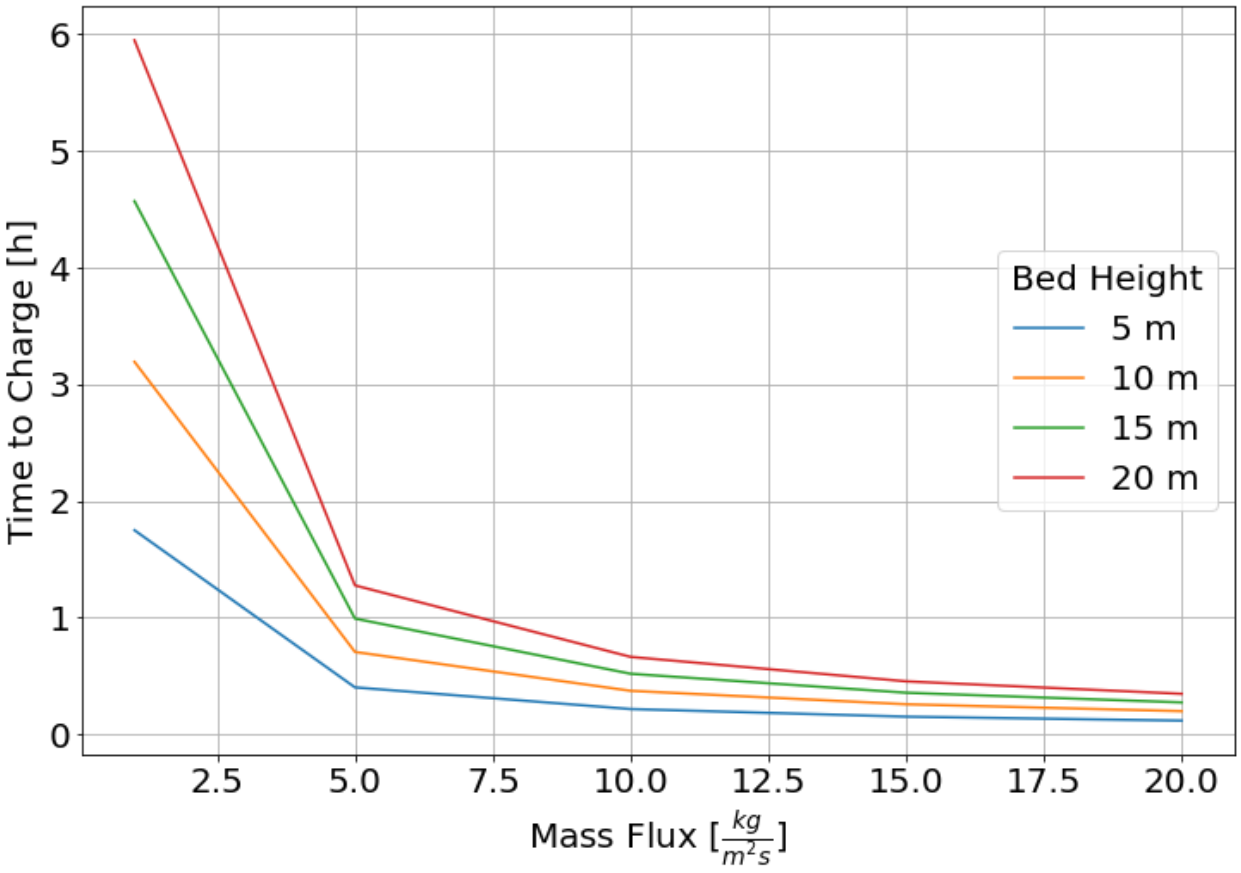

Figure 31. Time to charge crushed rock pile for different bed heights

6.2.5.4 Temperature Differential

The temperature differential of hot to cold is a parameter controlled by the designer. The highest temperature of the system is controlled by the steam temperature coming from the reactor which does not exceed 280°C for APR 1400. The lower temperature is chosen by the designer. Figure 32 shows the effect of the temperature differential on the charging time of the packed bed. The trench height is assumed to be 20 m and quartzite properties are used for crushed rock. Appendix B includes the results for Granite. A temperature drop value of 200°C is chosen for further analysis.

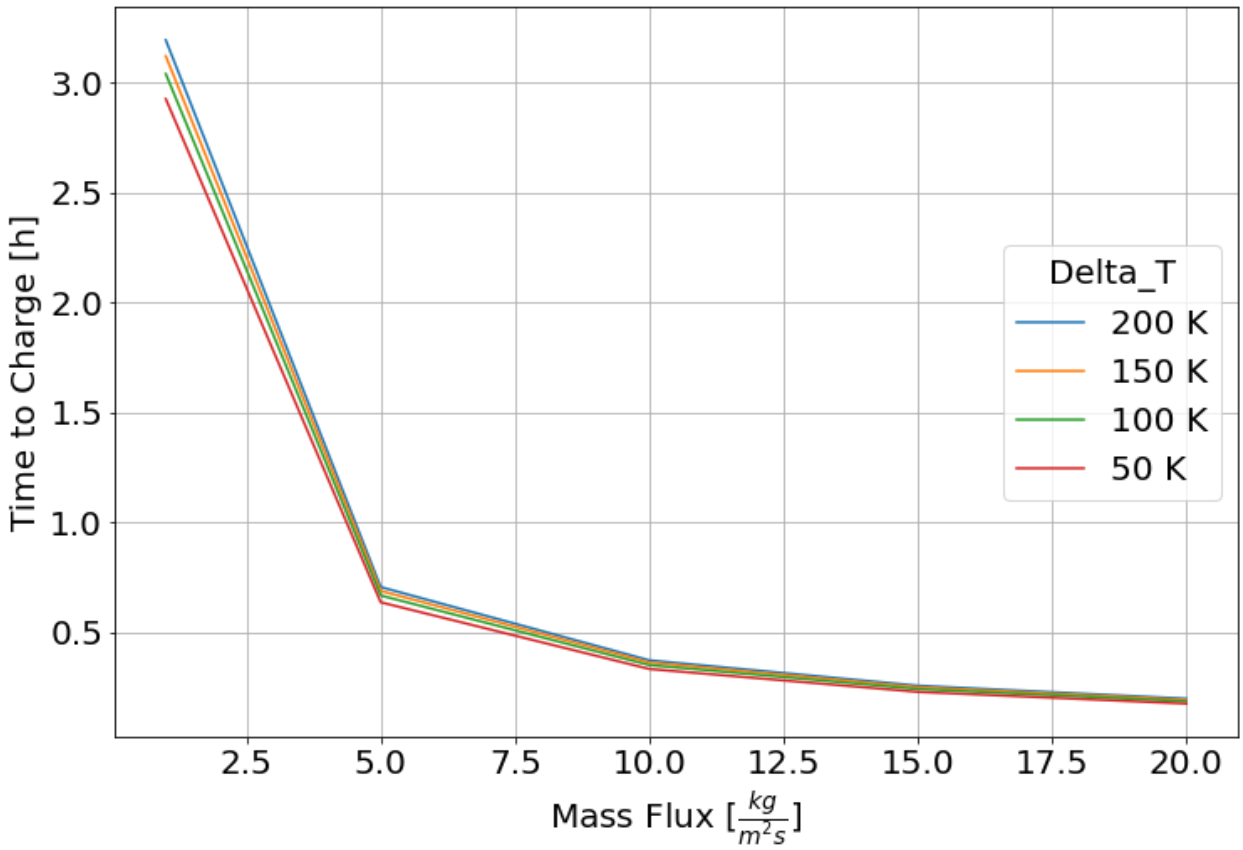

Figure 32. Time to charge crushed rock pile for different temperature differentials

6.2.5.4 Heat Transfer Fluid Velocity

The downward fluid velocity within a packed bed depends on the mass flux and the fluid density which in turn depends on the temperature of the fluid. Figure 33 shows the fluid velocity in the range of the 200°C temperature gradient for different mass flux values. The flow velocities are small over the full range of mass flow rates per unit area on top of the crushed rock, less than 5 cm/sec. In this first-generation model it was assumed the void fraction was filled with oil. A more accurate model would account for the gas being displaced by oil flow during startup and shutdown.

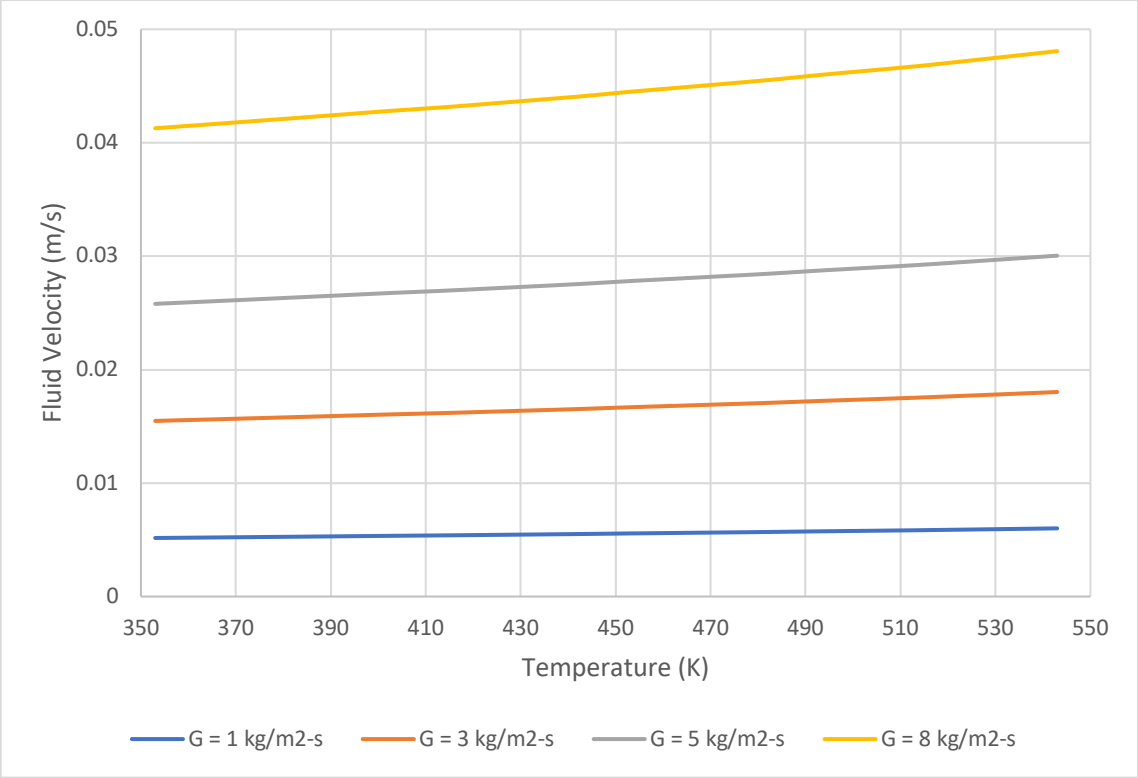

Figure 33. Fluid velocity for the operating temperature range of the storage system

6.3 Power Plant Integration and Sizing Energy Storage

CRUSH is characterized by multiple storage zones each chosen to be 25 m x 25 m in size. As some of the oil exiting the trench during charging is not fully cooled, one of the design goals is to limit the pumping of the hot exiting oil to one more section to reduce the cost and complexity of the system. The heat transfer model developed in a previous section for the crushed rock heat storage is used to calculate the time to charge per unit area of the system. The time to charge is the time required to fully heat one section of the trench. The mass flux is calculated based on the area of one section of the crushed rock system. The total oil flow rate is calculated as follows.

$$\dot{Q}_{tot} = \dot{m} C_f \Delta T \qquad \textit{Eq. 28}$$

Due to limitations of the minimum allowed steam generator feedwater temperature and pressure, the steam extraction from the steam generator of an APR 1400 is limited 20% (Amuda & Field, 2020). Therefore, the case study is 20% steam diverted from an APR 1400 unit. Equivalent to 800 MWth. The temperature differential is 200ºC. And properties of Thermion-66 are used. Thus, the total flow rate is calculated to be 1904 kg/s. One section of the trench is chosen to be 25 m x 25 m. therefore the mass flux is calculated as

$$G = \frac{\dot{m}}{A} = 3\ kg/(m^2 - s) \qquad \textit{Eq. 29}$$

The transient of the heat transfer between oil and rock is performed using the numerical model. Figure 34 shows the temperature profile of the crushed rock (Quartzite) and oil throughout the transient. It can be seen from the profile that at around 1.45 hours, hot oil start coming out from the bottom of the trench. This oil carries energy and will be pumped to the next section of the trench to pre heat it and fully cool the oil before return to be reheated. Appendix B includes the temperature profile transients for different temperature drops as well as for Granite.

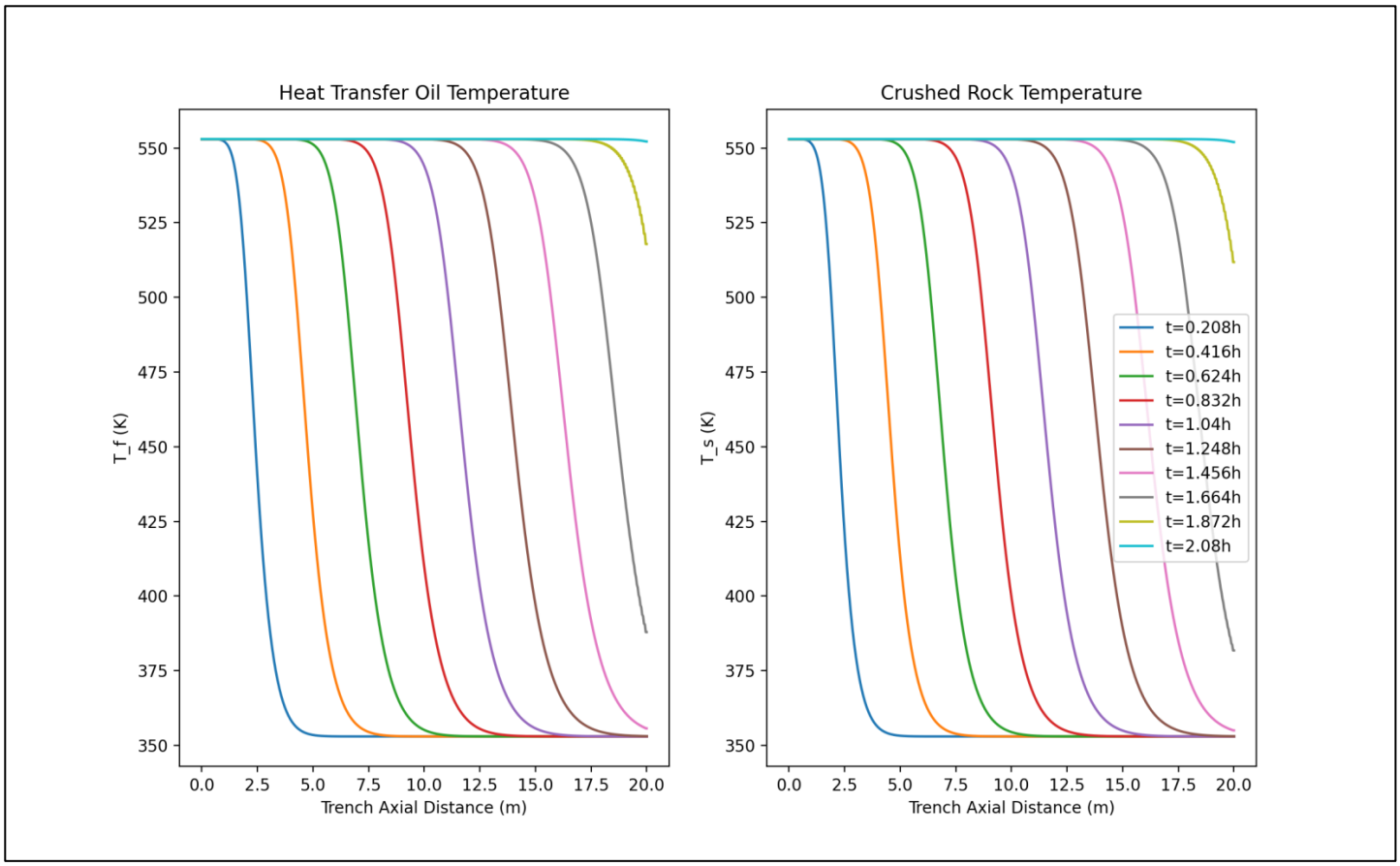

Figure 34. Temperature profile transient of heat transfer fluid and crushed rock for G=3 kg/m^2-s

The energy entering the system, the energy deposited in one section of the trench, and the energy pumped to the next section are calculated as follows.

$$E_{in} = \dot{m} C_f \Delta T \Delta t \qquad \textit{Eq. 30}$$

$$E_{dep} = V(1-\varepsilon)\rho_s C_s \Delta T \qquad \textit{Eq. 31}$$

$$E_{out} = E_{in} - E_{dep} \qquad \textit{Eq. 32}$$

The values calculated for one section (25 m x 25 m) of Quartzite and Granite are listed in Table 9 where E_{out} denotes the amount of heat pumped to the next section to pre heat. The results show that it will require the system to pump the oil coming out only once, as desired, to the next section where it will come out cold.

Table 9. Energy flow for one section (25 m x 25 m) of crushed rock storage

	Time to Charge (h)	$E_{in}\ (MWh)$	$E_{dep}\ (MWh)$	$E_{out}\ (MWh)$
Quartzite	2.08	1654	1153	501
Granite	2.60	2074	1497	576

The total volume of crushed rock is calculated as follows where Δt is the time to charge one section of the crushed rock pile, $\dot{Q}_{tot}$ is the heat diverted from the reactor, and ΔT is the temperature rise in the dry crushed rock.

$$V_{tot} = \frac{\dot{Q}_{tot} * \Delta t}{(1-\varepsilon)\rho_s C_s \Delta T} \qquad \textit{Eq. 33}$$

From equation 33 we find the total volume and number of sections required for charging 800 MWth of heat from the one reactor in 8 hours. The results are listed in Table 10. The values in Table 10 reflect the volume of the storage if heat is stored and discharged in a daily cycle. In the case of a weekend-weekday cycle where heat is stored during the weekend and discharged during the 5 days of the week, the volume of the storage is double the values in Table 10.

Table 10. Crushed rock storage volume requirements

	$V_{tot}\ (m^3)$	$A_{tot}\ (m^2)$	$\#\ of\ Sections$
Quartzite	69397	3470	5.5
Granite	53415	2671	4.3

7. Conclusion and Future Work

The traditional role of nuclear energy is providing baseload power. Through the coupling of heat storage to nuclear reactors, nuclear power can potentially penetrate new markets such as peak demand electricity—the traditional role of fossil fuels. This includes integrating nuclear and renewable systems in those locations with low-cost wind or solar. Throughout this thesis several potential benefits of nuclear heat storage to the energy market of the United Arab Emirates have been identified. Mainly, achieving climate change targets and insuring energy independence. Capacity Expansion Modeling through GenX has shown that in a carbon constrained market, coupling existing nuclear reactors in the UAE to heat storage allows for more gas turbine retirement as well as reduces the required renewable energy capacity to reach climate change target emissions.

A new very-low-cost heat storage system is proposed—CRUSH. CRUSH is at an early stage of development. This technology enables 100-GWh heat storage to address hourly to weekly needs for variable electricity from the base-load nuclear plants. Engineering analysis performed thorough out the thesis exhibited the option space and behavior of the CRUSH system.

Future work on CRUSH includes analytical as well as experimental work. From the analytical side, more accurate engineering models that account for the gas filling part of the void is essential to understanding the system behavior specially at the start up and shutdown of every cycle. Experimentally, a prototype of a crushed rock pile will allow for the study of the crushed rock and oil interactions as well as the estimating of oil hold up in the system. There is massive experience in heap leaching of copper and other ores. This is a water-based system involving mass transfer rather than heat transfer; but the theoretical, experimental and industrial experience provides guidance for understanding and scale-up of the CRUSH system.

Appendix A. Numerical Model (Python 3.9)

```python
import numpy as np
import matplotlib.pyplot as plt

print("starting")
Δx = 0.04
L = 20
T_0 = 80 + 273
T_1 = 80 + 273
Size = int(L / Δx)
Δt = 0.08
conv_cri = 279 + 273

# Initial Condition
T = T_0 * np.ones(Size)
T[0] = 280 + 273
Tother = T_1 * np.ones(Size)

# Create Matrices
d2dx2 = (
    -2 * np.diag(np.ones(Size))
    + np.diag(np.ones(Size - 1), k=1)
    + np.diag(np.ones(Size - 1), k=-1)
)
ddx = np.diag(np.ones(Size - 1), k=1) - np.diag(np.ones(Size - 1), k=-1)

m_dot = 3.0
Af = 1.0
dp = 2e-2
epsilon = 0.2
rho_s = 2500
Cs = 830
ks = (1 - epsilon) * 5.69

rho = lambda T: 1225.4 - 0.7281 * T
Cpf = lambda T: (0.483 + 0.0036 * T) * 1000
kf = lambda T: epsilon * (-2e-7 * T ** 2 + 5e-5 * T + 0.1153)
muf = lambda T: 8e18 * T ** (-8.147)

vf = lambda T: m_dot / rho(T) / Af / epsilon
Re = lambda T: rho(T) * dp * vf(T) / muf(T)
Pr = lambda T: Cpf(T) * muf(T) / kf(T)

hv = (
    lambda T: 6
    * (1 - epsilon)
    * kf(T)
    * (2 + 1.1 * Re(T) ** 0.6 * Pr(T) ** (1 / 3))
    / dp ** 2
)
```

```
55
56  T_history_1 = []
57  T_history_2 = []
58
59  import copy
60
61  t = 0
62
63  T_temp = copy.deepcopy(np.append(T, Tother, axis=0))
64
65  while True:
66      h2 = -np.diag(vf(T) / (2 * Δx))
67      h3 = -np.diag(hv(T) / (epsilon * rho(T) * Cpf(T)))
68      h_3 = np.diag(hv(T) / (epsilon * rho(T) * Cpf(T)))
69
70      g1 = ks / ((1 - epsilon) * rho_s * Cs) * np.diag(np.ones(Size)) / Δx ** 2
71      g3 = -np.diag(hv(T) / ((1 - epsilon) * rho_s * Cs))
72      g_3 = np.diag(hv(T) / ((1 - epsilon) * rho_s * Cs))
73
74      print(t, T_temp[-1])
75
76      Matrix11 = h2 @ ddx + h3
77      Matrix22 = g1 @ d2dx2 + g3
78
79      top = np.append(Matrix11, h_3, axis=1)[1:-1, :]
80      bottom = np.append(g_3, Matrix22, axis=1)[1:-1, :]
81
82      full = np.append(np.zeros((1, 2 * Size)), top, axis=0)
83      full = np.append(full, top[-1, :].reshape(1, 2 * Size), axis=0)
84      full = np.append(full, bottom[0, :].reshape(1, 2 * Size), axis=0)
85      full = np.append(full, bottom, axis=0)
86      full = np.append(full, bottom[-1, :].reshape(1, 2 * Size), axis=0)
87
88      dTdt = full @ T_temp
89
90      T_temp += Δt * dTdt
91      T = T_temp[:Size]
92
93      if T_temp[-1] >= conv_cri:
94          break
95
96      t += Δt
97
98      T_history_1.append(copy.deepcopy(T_temp[:Size]))
99      T_history_2.append(copy.deepcopy(T_temp[Size:]))
100
```

```
101
102   fig, (ax1, ax2) = plt.subplots(1, 2, figsize=(12, 8))
103
104   x = np.linspace(0, L, Size)
105   t = np.arange(0, t, Δt)
106
107   step = len(T_history_1) // 10
108   for t1, s, w in zip(
109       t[::step][1:-1], T_history_1[::step][1:-1], T_history_2[::step][1:-1]
110   ):
111       ax1.plot(x, s, label=f"t={round(t1/3600, 3)}h")
112       ax2.plot(x, w, label=f"t={round(t1/3600, 3)}h")
113
114   ax1.plot(x, T_history_1[-1], label=f"t={round(t[-1]/3600, 3)}h")
115   ax2.plot(x, T_history_2[-1], label=f"t={round(t[-1]/3600, 3)}h")
116
117   ax1.set_title(f"HTF G = {m_dot} kg/m2-s")
118   ax2.set_title(f"Solid G = {m_dot} kg/m2-s")
119   ax1.set_xlabel("Trench Axial Distance (m)")
120   ax2.set_xlabel("Trench Axial Distance (m)")
121   ax1.set_ylabel("T_f (K)")
122   ax2.set_ylabel("T_s (K)")
123   plt.legend(loc="right")
124   plt.show()
125
```

Model Verification for the case of : Granite, 20 m long trench, and 50 oC temperature drop

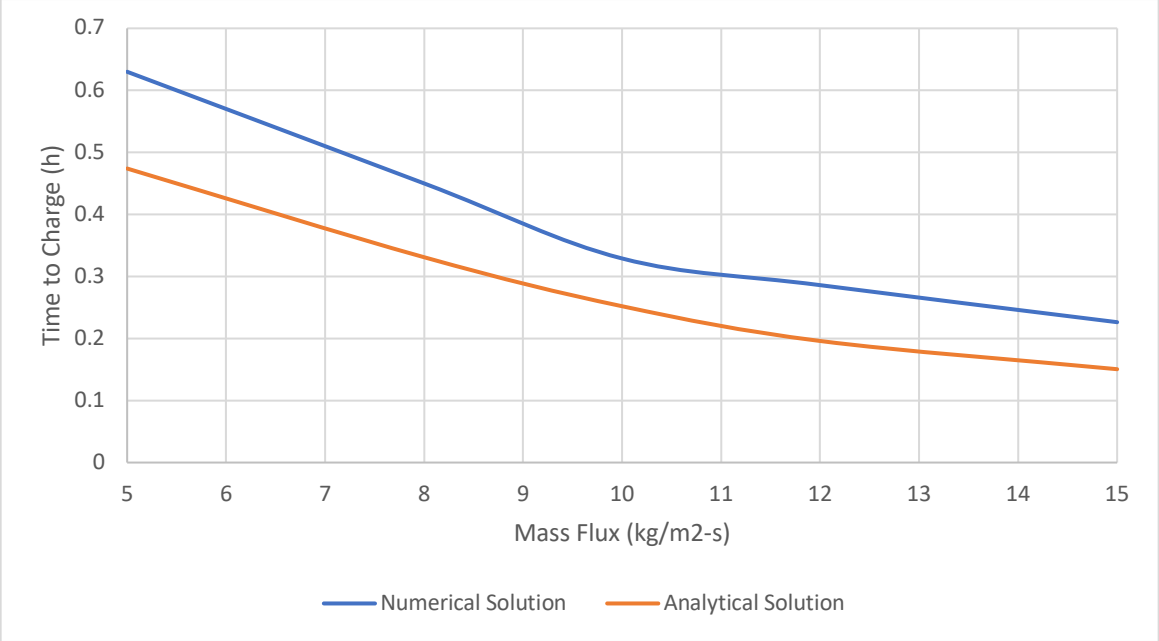

Appendix B. Supplementary Figures

Temperature gradient for 50°C drop (Quartzite)

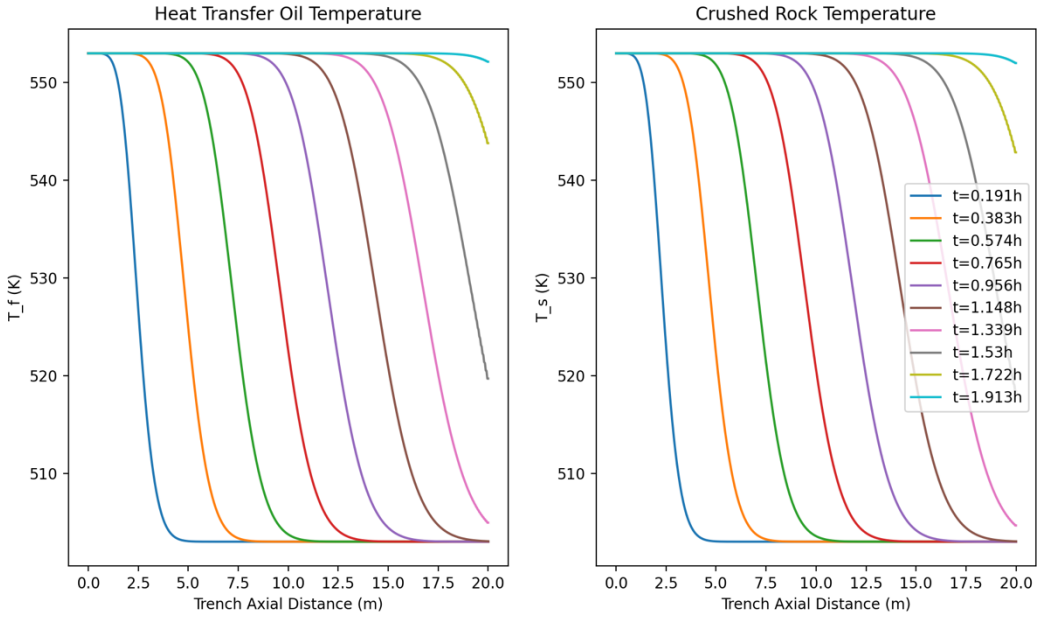

Temperature gradient for 100°C drop (Quartzite)

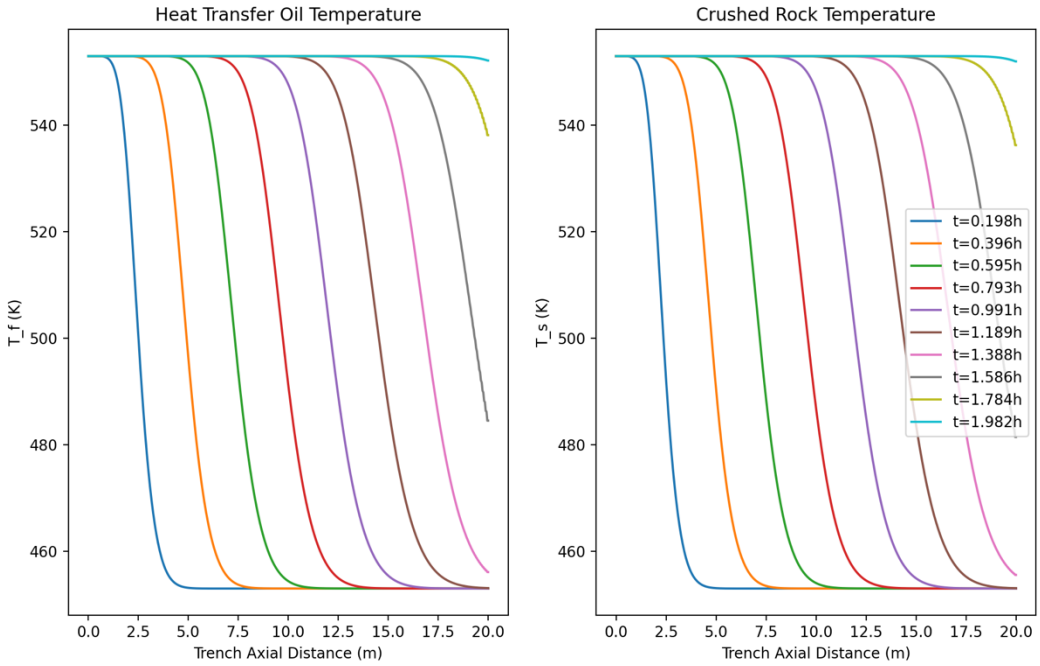

Temperature gradient for 150°C drop (Quartzite)

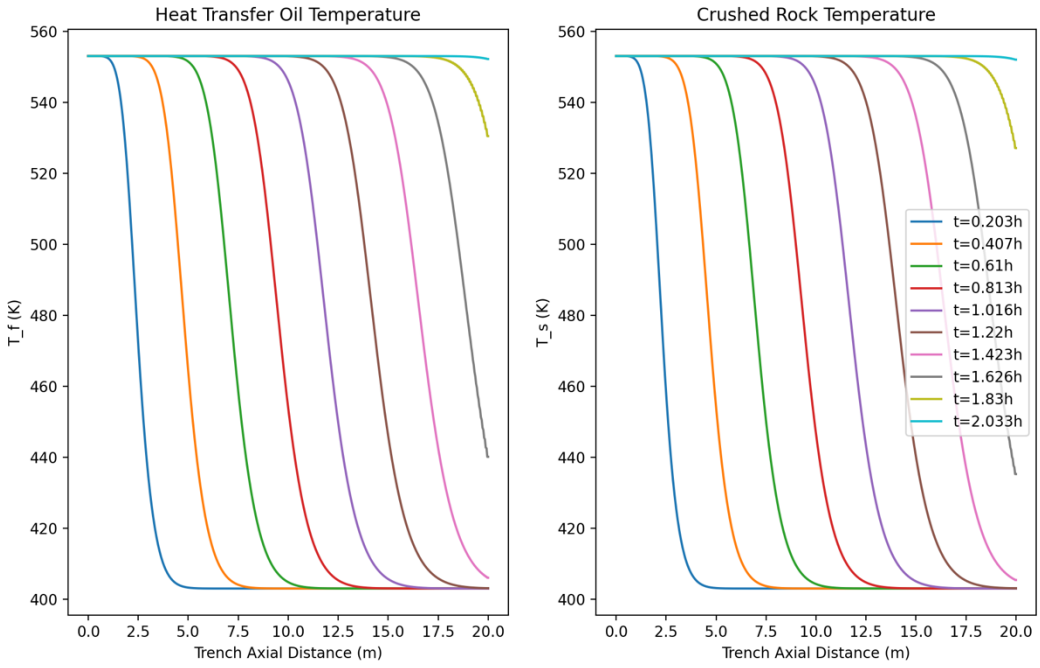

Temperature gradient for 200°C drop (Granite)

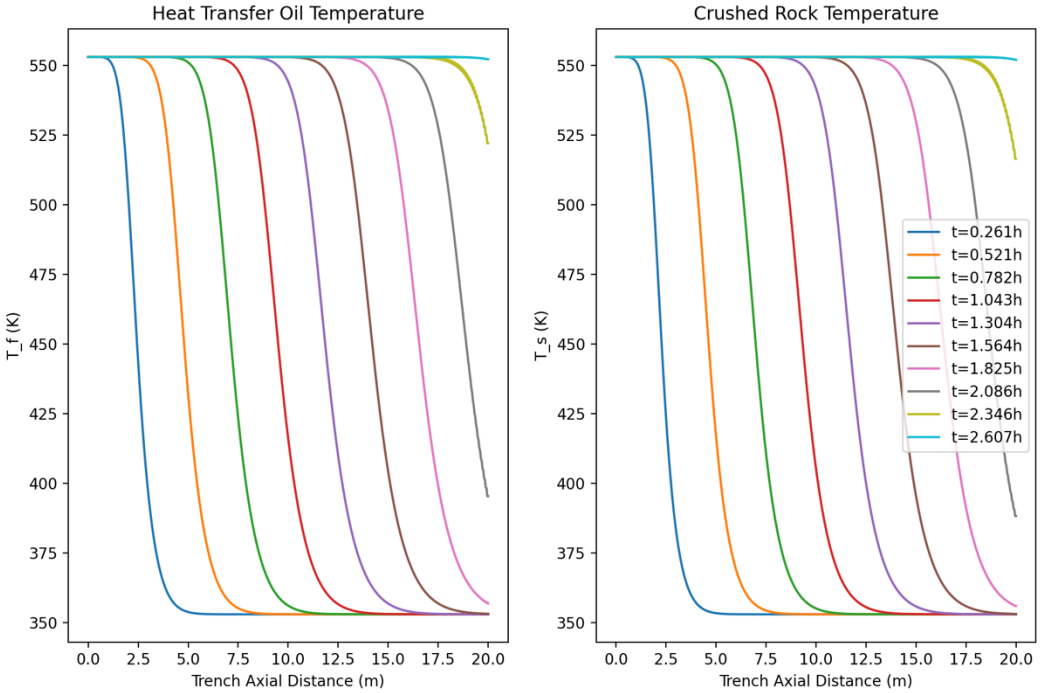

Bed height effect on Granite

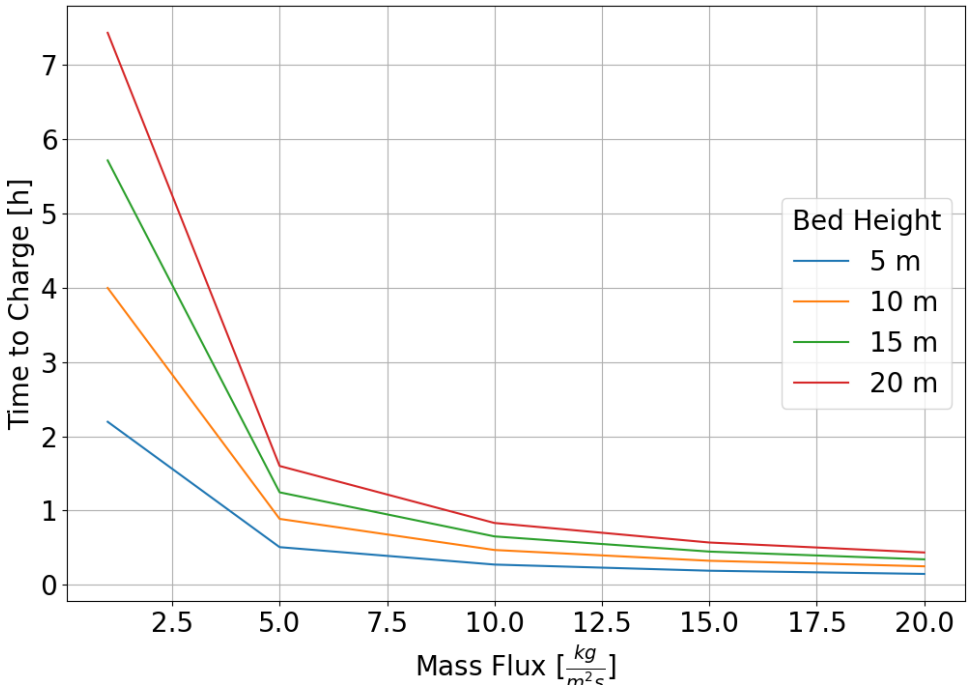

Temperature differential effect on Granite

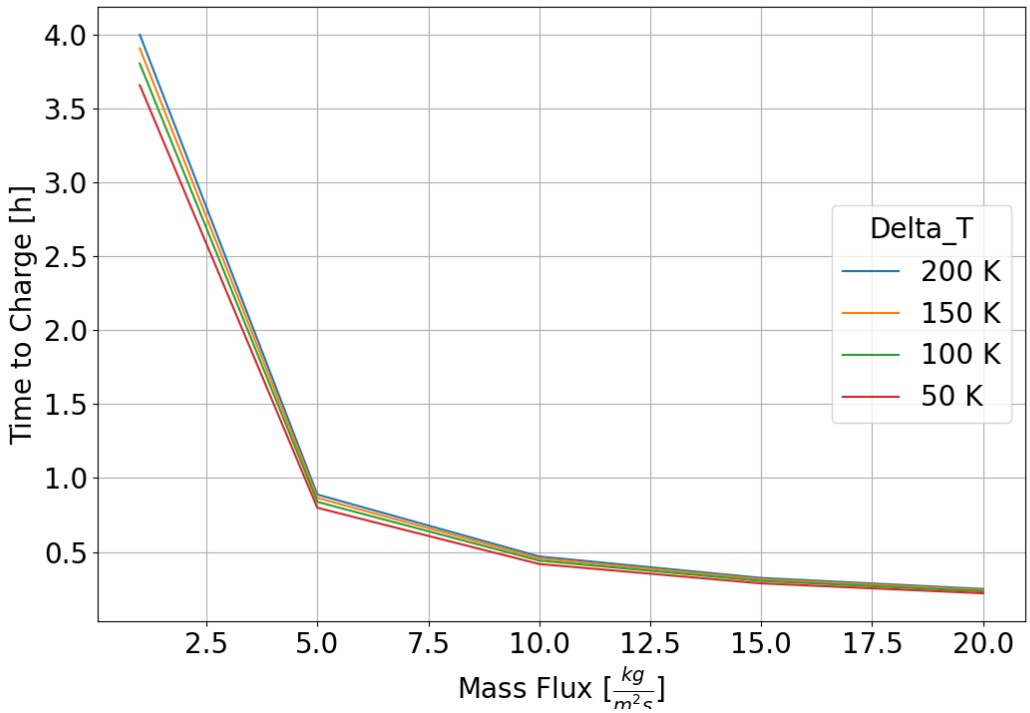

References

Abu Dhabi Transmission and Dispatch Company, "2018 Electricity Seven Year Planning Statement (2019-2025)." TRANSCO, 25 October 2018.

Allen K. G., (2010), Performance characteristics of packed bed thermal energy storage for solar thermal power plants. Master Thesis. University of Stellenbosch.

Amuda K. F. and Field R. M., "Proposed Heat Storage and Recovery Facility Designs for Korean Nuclear Power Plants using Ultra Large Floating Barge", Transactions of the Korean Nuclear Society Autumn Meeting, Goyang, Korea (October 23-25, 2019).

Awad, M., "Hydrogen Mobility in the UAE.", Khalifa University, October 2018.

Boardman R., Kim, J. S., Hancock, S., Hu, H., Frick, K., Wendt, D., Rabiti, C., Bragg-Sitton, S., Elgowainy, A., Weber, R., Holladay, J., "Evaluation of Non-electric Market Options for a Light-water Reactor in the Midwest.", Idaho National Laboratory, August 2019.

Bouffard, S.C., West-Sells, P.G., 2009. Hydrodynamic behavior of heap leach piles: Influence of testing scale and material properties. Hydrometallurgy 98, 136-142.

Carlson F., Davidson J. H., Parametric study of thermodynamic and cost performance of thermal energy storage coupled with nuclear power, Energy Conversion and Management, Volume 236, 2021, 114054, 0196-8904

Y. A. Cengel, Heat and Mass Transfer: A Practical Approach. Chapter 4. McGraw-Hill (2007).

CHAANAOUI M., VAUDREUIL S. AND BOUNAHMIDI T., "Benchmark of Concentrating Solar Power Plants: historical, current, and future technical and economic development," SEIT 2016, *Procedia Computer Science*, **83** (2016), 782-789

Cole, W. and Frazier, W., Cost Projections for Utility-Scale Battery Storage. Technical Report June 2019. National Renewable Energy Laboratory.

Eastman Company. Therminol 66 Technical Bulletin, Therminol Heat transfer fluids by Eastman company.

Eastman Company. Therminol VP-1 Technical Bulletin, Therminol Heat transfer fluids by Eastman company.

Field R. M., Ashong A. T., and Amuda K. F., "Nuclear Heat Storage & Recovery System Design for the APR1400." KEPCO International Nuclear Graduate School, 2019.

Forsberg, C.W., "Light Water Reactor Heat Storage for Peak Power and Increased Revenue: Focused Workshop on Near-Term Options" MIT-ANP-TR-170 (July 2017).

Ghorbani, Y., Franzidis, J.P., Petersen, J., 2016. Heap leaching technology – current state, innovations and future directions: A review. Minerals Processing and Extractive Metallurgy Review vol. 37 no 2, pp. 73-119.

Hoffmann J.F., Fasquelle T., Goetz V., Py X., A thermocline thermal energy storage system with filler materials for concentrated solar power plants: experimental data and numerical model sensitivity to different experimental tank scales, Appl. Therm. Eng. 100 (2016) 753–761.

Ilankoon I. M., Hydrodynamics of Unsaturated Particle Beds Pertaining to Heap Leaching, PhD Thesis, Imperial College, London, United Kingdom, 2012.

Irani F. N., Geology of the United Arab Emirates, Schlumberger Drilling and Measurements 2001.

IRENA, "Renewable Energy Prospects: United Arab Emirates REmap 2030 analysis." International Renewable Energy Agency, UAE, Apr. 2015.

IRENA, "Renewable Energy Market Analysis: GCC 2019." International Renewable Energy Agency, UAE, 2019.

Jenkins J. D. and Sepulveda N. A., "Enhanced Decision Support for a Changing Electricity Landscape: The GenX Configurable Electricity Resource Capacity Expansion Model." MIT Energy Initiative, MITEI-WP-2017-10, November 2017

Kluba, A.; Field, R. Optimization and Exergy Analysis of Nuclear Heat Storage and Recovery. Energies 2019, 12, 4205.

Lee, Y., Forsberg C. W., Driscoll M., and Sapie, B., June 13-17, 2010. "Options for Nuclear Geothermal Gigawatt-Year Peak Electricity Storage Systems, Proc. of ICAPP'10, San Diego.

Libby, C. et al., Electric Power Research Institute. Solar Thermocline Storage Systems. Preliminary Design Study. Final Report, June 2010.

McLauchlan N. R. (2018), Crushed Rock Thermal Energy Storage & Nuclear Technology: Option Space & Economic Impacts. Master Thesis. Massachusetts Institute of Technology.

MIT Energy Initiative, The Future of Nuclear Energy in a Carbon-Constrained World: An Interdisciplinary MIT Study, MIT Energy Initiative, Revision 1, 2018

Molina S., Haillot D., Deydier A., Bedecarrats J., Material screening and compatibility for thermocline storage systems using thermal oil, Appl. Therm. Eng. 146 (2019) 252–259.

Odenthal C. et. al., “Experimental and Numerical Investigation of a 4 MWh High Temperature Molten Salt Thermocline Storage System with Filler” Proc. of the SolarPaces, Daegu, South Korea (1-4, Oct 2019).

Orhan, M. F., Kahraman, H., and Binish S. B. "Approaches for integrated hydrogen production based on nuclear and renewable energy sources: Energy and exergy assessments of nuclear and solar energy sources in the United Arab Emirates." International Journal of Hydrogen Energy, June. 2016.

PELAY U., LUO L., FAN Y., STITOU D., ROOD M., “Technical data for concentrated solar power plants in operation, under construction and in project,” Data in Brief, Volume 13, August 2017, Pages 597-599

Pfenninger, Stefan and Staffell, Iain (2016). Long-term patterns of European PV output using 30 years of validated hourly reanalysis and satellite data. Energy 114, pp. 1251-1265

Sgouridis, S., Griffiths, S., Kennedy, S. W., Khalid, A., Zurita, N., “A Sustainable Energy Transition Strategy for United Arab Emirates: Evaluation of Options Using an Integrated Energy Model.”, Energy Strategy Reviews · June 2013.

Staden P. J., Effect of Scale of Operation on Heap Leaching Performance, PhD Thesis, University of Cape Town, South Africa. 3 May 2019.

Solar Thermal Energy News, The Shams 1 Solar Energy Center,” PROTERMOSOLAR (2015). http://helioscsp.com/the-shams-1-solar-energy-center/

Solar Thermal Energy News, “Concentrated solar power with steam turbines from Siemens,” PROTERMOSOLAR (2015) http://helioscsp.com/concentrated-solar-power-with-steam-turbines-from-siemens/

Wan Z., Wei J., Qaisrani M. A., Fang J., Tu N., “Evaluation on thermal and mechanical performance of the hot tank in the two-tank molten salt heat storage system”, Applied Thermal Energy, 167 (2020), 114775.

Xu C., Wang Z., He Y., Li X., Bai F., Sensitivity analysis of the numerical study on the thermal performance of a packed-bed molten salt thermocline thermal storage system, Appl. Energy 92 (2012) 65–75.